

Charged Higgs boson in the W^\pm Higgs channel at the Large Hadron Collider

Rikard Enberg^a, William Klemm^a, Stefano Moretti^b, Shoaib Munir^{a,c} and Glenn Wouda^a

^a *Department of Physics and Astronomy,
Uppsala University, Box 516, SE-751 20 Uppsala, Sweden.*

^b *School of Physics & Astronomy,
University of Southampton, Southampton SO17 1BJ, UK.*

^c *Asia Pacific Center for Theoretical Physics, San 31, Hyoja-dong,
Nam-gu, Pohang 790-784, Republic of Korea.*

Abstract

In light of the recent discovery of a neutral Higgs boson, H_{obs} , with a mass near 125 GeV, we reassess the LHC discovery potential of a charged Higgs boson, H^\pm , in the $W^\pm H_{\text{obs}}$ decay channel. This decay channel can be particularly important for a H^\pm heavier than the top quark, when it is produced through the $pp \rightarrow tH^\pm$ process. The knowledge of the mass of H_{obs} provides an additional handle in the kinematic selection when reconstructing a Breit-Wigner resonance in the $H_{\text{obs}} \rightarrow b\bar{b}$ decay channel. We consider some extensions of the Standard Model Higgs sector, with and without supersymmetry, and perform a dedicated signal-to-background analysis to test the scope of this channel for the LHC running at the design energy (14 TeV), for 300 fb^{-1} (standard) and 3000 fb^{-1} (high) integrated luminosities. We find that, while this channel does not show much promise for a supersymmetric H^\pm state, significant portions of the parameter spaces of several two-Higgs doublet models are testable.

[†]E-mails:

Rikard.Enberg@physics.uu.se,

William.Klemm@physics.uu.se,

S.Moretti@soton.ac.uk,

S.Munir@apctp.org,

Glenn.Wouda@physics.uu.se.

1 Introduction

A charged Higgs boson, H^\pm , is predicted in many models of new physics, with and without Supersymmetry (SUSY). The observation of a H^\pm at the Large Hadron Collider (LHC) is thus expected to provide concrete evidence of physics beyond the Standard Model (SM). The strategies for such searches depend on the mass, m_{H^\pm} , of the charged Higgs boson. A H^\pm lighter than the top quark can be produced in $t \rightarrow H^+b$ and $\bar{t} \rightarrow H^-\bar{b}$ decays, where the top quarks are produced in pairs in $q\bar{q}$ annihilation and gg fusion (see [1] and references therein). When $m_{H^\pm} > m_t - m_b$, $bg \rightarrow tH^-$ and $gg \rightarrow tH^-\bar{b}$ are by far the dominant production processes.¹ As for the decays, $H^\pm \rightarrow \tau\nu$ ² is the dominant mode as long as $m_{H^\pm} < m_t + m_b$, beyond which $H^\pm \rightarrow tb$ becomes the leading decay channel with branching ratio (BR) approaching unity.

The Minimal Supersymmetric Standard Model (MSSM) is an example of a scenario predicting charged Higgs states. In fact, it contains a total of five physical Higgs states. Among the neutral ones are included two CP-even states, with the lighter one denoted by h and the heavier by H , a CP-odd state, A , and there is also a charged pair H^\pm . The detection of an MSSM H^\pm lighter than the top quark is rather straightforward for a wide range of $\tan\beta$ (where $\tan\beta \equiv v_2/v_1$, with v_1 and v_2 being the vacuum expectation values (VEVs) of the two Higgs doublet fields Φ_1 and Φ_2). $H^\pm \rightarrow \tau\nu$ is the dominant decay mode of such a H^\pm for all $\tan\beta$. For $m_{H^\pm} > m_t + m_b$, the large reducible and irreducible backgrounds make the search for H^\pm in the tb decay mode notoriously difficult [10] (see [11, 12] for experimental simulations). However, some studies [13, 14] concluded that the LHC discovery potential of a H^\pm state with mass $\lesssim 600$ GeV is satisfactory in this decay channel, but only for very small, $\lesssim 1.5$, or very large, $\gtrsim 30$, values of $\tan\beta$. It has also been shown [15] that the $H^\pm \rightarrow \tau\nu$ decay mode can be used at the LHC even for $200 \text{ GeV} < m_{H^\pm} < 1 \text{ TeV}$ provided $\tan\beta \gtrsim 3$. In fact, if the distinctive τ -polarisation [16] is used, the $H^\pm \rightarrow \tau\nu$ channel can provide at least as good a heavy H^\pm signature as the $H^\pm \rightarrow tb$ decay mode (for the large $\tan\beta$ regime [17]).

At the LHC several searches have been carried out for H^\pm 's lighter as well as heavier than the top quark. The CMS collaboration has recently released exclusion limits [18] for a H^\pm lying in the 180 GeV – 600 GeV mass range. That study assumes $gg \rightarrow tH^-\bar{b}$ production and $H^\pm \rightarrow tb$ and $H^\pm \rightarrow \tau\nu$ decay modes and is based on 19.7 fb^{-1} of data collected at $\sqrt{s} = 8 \text{ TeV}$. An earlier analysis [19] based on the same dataset provided exclusion limits in the $H^\pm \rightarrow \tau\nu$ decay channel for $80 \text{ GeV} < m_{H^\pm} < 160 \text{ GeV}$, assuming $t\bar{t} \rightarrow H^\pm W^\pm b\bar{b}$ production, and for $180 \text{ GeV} < m_{H^\pm} < 600 \text{ GeV}$, using the inclusive $pp \rightarrow tH^-(b)$ production mode. The same production and decay modes have also been analysed by the ATLAS collaboration [20] based on 19.5 fb^{-1} of data at $\sqrt{s} = 8 \text{ TeV}$, providing exclusion limits for $80 \text{ GeV} < m_{H^\pm} < 160 \text{ GeV}$ and $180 \text{ GeV} < m_{H^\pm} < 1 \text{ TeV}$. In an earlier ATLAS study [21] based on 4.7 fb^{-1} of data at $\sqrt{s} = 7 \text{ TeV}$, the $H^\pm \rightarrow cs$ decay channel has also been probed for H^\pm lying in the mass range 90 GeV – 150 GeV.

Note, however, that the two dominant decay channels mentioned above, i.e., tb and $\tau\nu$, leave the $1.5 \lesssim \tan\beta \lesssim 3$ window virtually unexplorable for a H^\pm heavier than the top quark in the MSSM. Importantly, it is for such small values of $\tan\beta$ that the $\text{BR}(H^\pm \rightarrow W^\pm h)$ becomes sizeable, reaching the percent level. The detectability of a Supersymmetric H^\pm in the $W^\pm h$ decay channel was studied in [22], where it was noted that a H^\pm with mass around 200 GeV could be detectable at

¹These are in fact one and the same process, describing the underlying dynamics in two different regimes, when combined with the parton distribution functions (pdfs). A combination of these two modes with a subtraction of the common terms is the preferred computational method, as described originally in [2, 3] for neutral Higgs boson production and adapted later in [4, 5] for charged Higgs boson production, with an implementation of the latter made available in [6, 7]. (Also, see Refs. [8, 9] for a discussion on the QCD accuracy at the next-to-leading order (NLO).) Further aspects in this context relevant to our analysis can be found in Sec. 5 below.

²We do not distinguish between fermions and anti-fermions when their identity is either unspecified or can be inferred from the context.

the LHC with $\sqrt{s} = 14 \text{ TeV}$ and $\mathcal{L} = 300 \text{ fb}^{-1}$, for $\tan\beta = 2-3$. But there are two caveats. First, in these studies the mass of h was not fixed to the value eventually measured at the LHC. Second, such low values of $\tan\beta$ may at first glance appear to be excluded by the LEP2 Higgs boson searches [23], particularly for low $m_A \sim 100 \text{ GeV}$. However, as discussed in [24], the LEP limit typically assumes a SUSY-breaking scale, M_{SUSY} , in the vicinity of 1 TeV, which should be relaxed owing to the fact that SUSY remains undiscovered, implying a significantly higher breaking scale. Now, a realistic SUSY model ought to contain a Higgs boson, H_{obs} , consistent with the one discovered at the LHC [25] and hence satisfying the ‘observational constraint,’ $122 \text{ GeV} \lesssim m_{H_{\text{obs}}} \lesssim 128 \text{ GeV}$, which supersedes the LEP limit. The large allowed mass window is to take into account the theoretical uncertainties in the calculation of the H_{obs} mass in the model. All such aspects clearly need to be re-assessed in light of the latest experimental results.

Besides the above observational constraint on the mass of the Higgs boson, the LHC measurements of its signal strengths in various production and decay channels also strongly constrain the parameter space of the MSSM wherein a H^\pm , potentially visible via the $W^\pm H_{\text{obs}}$ decay, can be obtained. In its singlet-extension, the Next-to-Minimal Supersymmetric Standard Model (NMSSM), the mass of the SM-like Higgs boson satisfying the mentioned mass constraint can be achieved in a more natural way, without requiring large radiative corrections from the stop sector. Such a Higgs boson, in fact, favours a lighter H^\pm , as we shall discuss in detail below. Moreover, in this model, which contains a total of 5 neutral Higgs states, the role of H_{obs} can be played by the any of the two lightest CP-even Higgs bosons, H_1 or H_2 , alternatively [26].

If one leaves aside SUSY, one of the simplest non-trivial extensions of the SM is represented by a 2-Higgs doublet model (2HDM), which contains two Higgs doublets with different Yukawa assignments (see [27] for a review). Notably, this structure (albeit limited to one specific Yukawa configuration) is necessary in the MSSM, implying that the Higgs spectrum in a CP-conserving 2HDM is the same as in the MSSM, containing three neutral Higgs bosons and a charged pair. However, the absence of SUSY relations amongst the Higgs boson masses allows much more freedom to alternatively identify the discovered SM-like Higgs state with either of the two CP-even Higgs bosons of a 2HDM. Depending on the way the Higgs doublets are assigned charges under a Z_2 symmetry imposed in order to avoid large flavour-changing neutral currents (FCNCs), the 2HDMs are generally divided into four different types. In the ‘aligned’ 2HDM [28] (A2HDM), instead of the Z_2 symmetry, a Yukawa-alignment is enforced in order to prevent large FCNCs.

From the point of view of H^\pm searches, results obtained in the MSSM can be easily translated to the case of a 2HDM Type II, as long as SUSY states are very heavy, i.e., decoupled [29]. This is somewhat more involved in the case of the other three ordinary Types and the A2HDM, although still possible (see [30] and [31], respectively). Some dedicated analyses of the 2HDMs to constrain them using the latest data from the LHC have also been performed recently [32]. The key phenomenological difference in the 2HDMs from the SUSY models in general, and the MSSM and NMSSM in particular, is that there are no light SUSY particles to provide cancellations (induced by the different spin statistics between SM and SUSY states) in low energy observables, chiefly from flavour dynamics. It is in fact the latter (e.g., limits on the $Z \rightarrow b\bar{b}$ and $b \rightarrow s\gamma$ decays) that generally produce severe constraints on the mass of H^\pm in the standard 2HDMs, pushing it to be larger than the top quark mass [33]. In the A2HDM, however, one can obtain $m_{H^\pm} < m_t$ in a viable region of the parameter space [34].

In this article we analyse the possibility of establishing a $H^\pm \rightarrow W^\pm H_{\text{obs}}$ signal in the next LHC run in all the models mentioned above, which are those where some relevance of such a decay has been established in the literature previously. We exploit the requirement on H_{obs} to have a mass around 125 GeV, so that the m_{H^\pm} range accessible via this signature starts at about 200 GeV and extends to nearly 500 GeV, as for heavier masses the tH^\pm production cross section becomes too

low. We first discuss the consistency of the corresponding regions of the parameter spaces of these models with the current Higgs boson data from the LHC. We further assess the effects of imposing constraints from b -physics and, in the case of SUSY models, cold dark matter (DM) relic density measurements. We also carry out a model-independent detector-level analysis of the expected LHC sensitivity in the $H^\pm \rightarrow W^\pm H_{\text{obs}}$ channel with $\sqrt{s} = 14$ TeV. In doing so, we exploit the knowledge of the mass of H_{obs} , which will result in a substantial improvement in the efficiency of previously advocated [22] kinematical selections for the extraction of the signature of concern here, which we use for guidance. We then compare the sensitivities expected for various integrated luminosities at the LHC with the cross sections obtainable for this channel in each model considered in the presence of the aforementioned experimental constraints.³ It will be the interplay between the improved selection and the reduced parameter space available following the Higgs boson discovery (with respect to the setups assumed in earlier analyses of the H^\pm decay mode considered here) that will determine the actual situation at present.

The article is organised as follows. In Sec. 2 we will discuss the production and decay mechanisms of the H^\pm considered in our analysis. In Sec. 3, we will discuss some salient features of the models analysed. In Sec. 4 we will provide some details of the scans of the parameter spaces of these models and of the experimental constraints imposed in our study. In Sec. 5 we will explain our signal-to-background analysis. In Sec. 6 we will present our results and in Sec. 7 our conclusions.

2 Production and decay of H^\pm

The dominant production process at the LHC for a H^\pm heavier than the top quark is its associated production with a single top, with the relevant subprocesses being $bg \rightarrow tH^-$ and $gg \rightarrow t\bar{b}H^-$ (plus charge conjugated channels). The division between these two subprocesses is not clear-cut. The gg amplitude can be seen as a tree-level contribution to the NLO amplitude that includes a virtual b -quark, with the bg process making the LO amplitude. In the gg process we may view the b -quarks (the virtual b and the emitted b) as resulting from a splitting of the gluon and the corresponding amplitude contains the exact kinematics of this splitting. In the bg process the b -quark instead comes from the parton distribution of the proton. The b -quark is then a collinear parton arising from a splitting in the evolution of the pdfs. This contribution to the amplitude contains a collinear approximation of the kinematics and also a resummation of large logarithms in the factorisation scale that is not present in the gg amplitude.

When calculating the cross section for $pp \rightarrow tH^\pm + X$ the bg and gg contributions to the amplitude cannot be added naively because that would result in double counting between the two contributions. There is a correct procedure to compute the total cross section [36], but it does not generalise to the differential cross section needed for Monte Carlo (MC) simulations. In Ref. [6] a method for event generation without double counting was introduced, and an add-on, called MATCHIG, to the event generator Pythia6 [37] was constructed. In this framework events are generated both for the bg and gg processes and for the double-counting contribution. Events corresponding to the double counting have negative weights and should be subtracted from the positive weighted bg and gg processes. We have used MATCHIG in our simulations.⁴

The process $pp \rightarrow tH^\pm + X$ has also been calculated at NLO and has been implemented [38] in the POWHEG BOX MC framework [39], which includes matching to parton showers. At NLO the bg and gg contributions are both part of the amplitude. It has also been implemented [40] in the MC@NLO framework [41]. In [38] it was shown that the MATCHIG program produces very

³See [35] for a similar analysis for some Type II 2HDM benchmark points.

⁴The process $bg \rightarrow tH^-$ already exists in the publicly available Pythia package.

similar kinematical distributions to the POWHEG implementation except at very large transverse momentum, $p_T > 200$ GeV of the tH^\pm pair. The overall normalisation is, however, larger for the NLO calculations. The ratio between the total cross sections at NLO and LO depends on the model parameters via the mass spectrum, but for an example choice of 2HDMs it was found to be around a factor 2 for the Tevatron energies and a factor 1.4 for the LHC energies [38]. We do not consider this NLO enhancement of the signal in this paper for consistency, as we are only able to simulate the backgrounds at LO, but one should bear in mind that our quoted sensitivities may be somewhat stronger if NLO effects were systematically taken into account.

The spin/colour summed/averaged squared amplitude for the $gb \rightarrow tH^-$ production process is given by [42]

$$|\overline{\mathcal{M}}|^2 = \frac{g_{qH^\pm}^2}{2m_W^2} \frac{g_s^2 g_2^2}{4N_c} |V_{tb}|^2 \frac{(u - m_{H^\pm}^2)^2}{s(m_t^2 - t)} \left[1 + 2 \frac{m_{H^\pm}^2 - m_t^2}{u - m_{H^\pm}^2} \left(1 + \frac{m_t^2}{t - m_t^2} + \frac{m_{H^\pm}^2}{u - m_{H^\pm}^2} \right) \right], \quad (1)$$

where g_s and g_2 are the $SU(3)_C$ and $SU(2)_L$ gauge couplings, $N_C = 3$ is the number of colours and V_{tb} is the relevant CKM matrix element. See Refs. [14] and [43] for the $gg \rightarrow tH^- \bar{b}$ amplitudes and graphs. The total cross section is proportional to the coupling $g_{qH^\pm}^2$, as noted in the equation above, which is the only model dependent factor for a given m_{H^\pm} . This factor depends on the masses, m_t and m_b , of the t and b quarks, respectively, as well as the parameter $\tan \beta$, and will be discussed in the next section for each model considered here. As shown in [6], the total cross section for a charged Higgs mass above m_t is actually well-approximated by the bg cross section. However, since the bg and the gg contributions lead to different kinematical distributions in the MC simulations, as noted above, we included both these contributions in our MC simulations.

Finally, as noted in the Introduction, this study aims to exploit the $H^\pm \rightarrow W^\pm H_{\text{obs}}$ decay channel at the LHC. Of relevance for this particular process is the coupling of H^\pm to a generic neutral Higgs boson, H_i , and the W boson, given by

$$g_{H_i H^\pm W^\mp} = \frac{g_2}{2} (\cos \beta S_{i2} - \sin \beta S_{i1}), \quad (2)$$

where S_{i1} and S_{i2} are the elements of the mixing matrix that diagonalises the CP-even Higgs mass matrix in the model. It is clear that this coupling depends strongly on $\tan \beta$, both explicitly and through the elements S_{i1} and S_{i2} , (except in the A2HDM, as will be explained later) making the $H^\pm \rightarrow W^\pm H_{\text{obs}}$ decay process highly sensitive to this parameter.

3 The models

3.1 Supersymmetric models

The Supersymmetric models considered here contain two Higgs doublets, Φ_1 and Φ_2 , which make the scalar components of the superfields \widehat{H}_d and \widehat{H}_u , respectively. The field Φ_1 is needed for generating the masses of the d -type quarks and leptons and Φ_2 those of the u -type quarks. The coupling of the charged Higgs boson to the quarks, defined in Eq. (1) as the factor $g_{qH^\pm}^2$, is given in these models as

$$g_{qH^\pm}^2 = m_b^2 \tan^2 \beta + m_t^2 \cot^2 \beta. \quad (3)$$

Thus the amplitude for the $gb \rightarrow tH^-$ process is maximal for either small or large $\tan \beta$.

- **MSSM**

The MSSM Superpotential, from which the scalar potential is derived, is given as

$$W_{\text{MSSM}} = h_u \widehat{Q} \cdot \widehat{H}_u \widehat{U}_R^c + h_d \widehat{H}_d \cdot \widehat{Q} \widehat{D}_R^c + h_e \widehat{H}_d \cdot \widehat{L} \widehat{E}_R^c + \mu \widehat{H}_u \cdot \widehat{H}_d, \quad (4)$$

where \widehat{Q} , \widehat{U}_R^c , \widehat{D}_R^c , \widehat{L} and \widehat{E}_R^c are the quark and lepton superfields and h_u , h_d and h_e are the corresponding Yukawa couplings. In this model, the mass of H^\pm is given at LO as

$$m_{H^\pm}^2 = m_A^2 + m_W^2, \quad (5)$$

where m_W is the mass of the W boson. In order to allow the $H^\pm \rightarrow W^\pm H_{\text{obs}}$ decay, one requires $m_{H^\pm} > m_{H_{\text{obs}}} + m_W$, which translates into the requirement $m_A \gtrsim 190 \text{ GeV}$. In the MSSM, under such a condition, the tree-level mass of the SM-like Higgs boson, H_{SM} , has an upper limit

$$m_{H_{\text{SM}}}^2 \leq m_Z^2 \cos^2 2\beta, \quad (6)$$

where m_Z is the mass of the Z boson. Therefore, if the H_{SM} is identified with the H_{obs} and hence required to have a mass close to 125 GeV in accordance with the LHC measurement, a large value of $\tan \beta$ is necessary. Furthermore, the absence of any significant deviations of the signal strengths of the H_{obs} from the SM expectations so far [44] seems to be pushing the MSSM towards the so-called ‘decoupling regime’. This regime corresponds to $m_A \gtrsim 150 \text{ GeV}$ for $\tan \beta \gtrsim 10$ and yields SM-like couplings of the H_{SM} , in addition to a maximal tree-level mass, as noted above. The net effect of all these observations is that a H^\pm with mass greater than 200 GeV and a H_{SM} with the correct mass and SM-like couplings can be obtained simultaneously only for large $\tan \beta$. However, according to Eqs. (2) and (3), $\tan \beta \sim 10$ not only diminishes the $\text{BR}(H^\pm \rightarrow W^\pm H_{\text{SM}})$ but also the $gb \rightarrow tH^-$ cross section.

The complete MSSM contains more than 120 free parameters in addition to those of the SM. In its phenomenological version, the pMSSM, one assumes the matrices for the sfermion masses and for the trilinear scalar couplings to be diagonal, which reduces the parameter space of the model considerably. Here, since we are mainly concerned with the Higgs sector of the model, we further impose the following mSUGRA-inspired (where mSUGRA stands for minimal supergravity) universality conditions:

$$\begin{aligned} m_0 &\equiv M_{Q_{1,2,3}} = M_{U_{1,2,3}} = M_{D_{1,2,3}} = M_{L_{1,2,3}} = M_{E_{1,2,3}}, \\ m_{1/2} &\equiv 2M_1 = M_2 = \frac{1}{3}M_3, \\ A_0 &\equiv A_t = A_b = A_\tau, \end{aligned} \quad (7)$$

where $M_{Q_{1,2,3}}$, $M_{U_{1,2,3}}$, $M_{D_{1,2,3}}$, $M_{L_{1,2,3}}$ and $M_{E_{1,2,3}}$ are the soft masses of the sfermions, $M_{1,2,3}$ those of the gauginos and $A_{t,b,\tau}$ the soft trilinear couplings. This leaves us with a total of six free parameters, namely m_0 , $m_{1/2}$, A_0 , m_A , $\tan \beta$ and the Higgs-higgsino mass parameter μ .

• NMSSM

The NMSSM [45, 46, 47] (see, e.g., [48, 49] for reviews) contains a singlet Higgs field in addition to the two doublet fields of the MSSM. The scale-invariant Superpotential of the NMSSM is written as

$$W_{\text{NMSSM}} = \text{MSSM Yukawa terms} + \lambda \widehat{S} \widehat{H}_u \cdot \widehat{H}_d + \frac{\kappa}{3} \widehat{S}^3, \quad (8)$$

where \widehat{S} is the additional Higgs singlet Superfield and λ and κ are dimensionless Yukawa couplings. The introduction of the new singlet field results in a total of five neutral Higgs mass eigenstates

and a H^\pm pair, after rotating away the Goldstone bosons. In the NMSSM, the MSSM upper limit on the tree-level mass of the SM-like Higgs boson, given in Eq. (6), gets modified as

$$m_{H_{\text{SM}}}^2 \leq m_Z^2 \cos^2 2\beta + \frac{\lambda^2 v^2 \sin^2 2\beta}{2} - \frac{\lambda^2 v^2}{2\kappa^2} \left[\lambda - \sin 2\beta \left(\kappa + \frac{A_\lambda}{\sqrt{2}s} \right) \right]^2, \quad (9)$$

where $v \equiv \sqrt{v_1^2 + v_2^2} = 246 \text{ GeV}$, s is the VEV of the singlet field and A_λ is the soft SUSY-breaking parameter corresponding to the coupling λ . Clearly, for large values of λ and small $\tan\beta$, the second term in the above equation gives a significant positive contribution to the H_{SM} mass.

The mass expression for H^\pm in the NMSSM is given as

$$m_{H^\pm}^2 = m_A^2 + m_W^2 - \frac{v^2 \lambda^2}{2}, \quad (10)$$

where m_A^2 is, in contrast with the MSSM, the diagonal entry $[M_A^2]_{11}$ of the pseudoscalar mass matrix M_A^2 of the model, given by

$$m_A^2 = [M_A^2]_{11} = \frac{\sqrt{2}\lambda s}{\sin 2\beta} \left(A_\lambda + \frac{\kappa s}{\sqrt{2}} \right). \quad (11)$$

Again, for a given value of $\tan\beta$, the negative third term in Eq. (10) results in a smaller $m_{H^\pm}^2$ in the NMSSM compared to that in the MSSM, where it is given by the first two terms only. This negative contribution increases with the size of λ .

A crucial observation here is that a large λ , necessary to obtain sufficiently small m_{H^\pm} , has the dual advantage of enhancing also the tree-level mass of H_{SM} , as noted above. Such a scenario is therefore more natural than the one with a very MSSM-like H_{SM} , since a much smaller amount of fine-tuning is required to achieve the correct Higgs boson mass via radiative corrections. But large λ also implies a substantial singlet component in H_{SM} , which could result in significantly reducing its couplings to fermions and gauge bosons compared to those of the SM Higgs boson. However, recent studies [26] have shown that, for large λ and small $\tan\beta$, the H_{SM} of the model, which can correspond to either H_1 or H_2 , can still be consistent with the LHC Higgs boson data. The signal strength of H_{SM} in the $\gamma\gamma$ decay channel in such a scenario can in fact be much larger than that of a SM-like Higgs boson, owing to a reduction in the $\text{BR}(H_{\text{SM}} \rightarrow b\bar{b})$ compared to the true SM case. We point out here that, as in the MSSM, the H_{SM} in the NMSSM will also be identified with H_{obs} , since it is assumed to be the Higgs boson observed at the LHC.

The phenomenological version of the NMSSM that we study here contains three new parameters in addition to those of the pMSSM, mentioned earlier, with μ replaced by $\mu_{\text{eff}} (\equiv \lambda s)$ and m_A traded for A_λ . These include λ , κ and A_κ , the latter being a dimensionful coupling originating in the SUSY-breaking part of the Higgs potential.

3.2 2HDMs

A generic non-Supersymmetric 2HDM is defined by its scalar potential and its Yukawa couplings. The two Higgs doublets in such a model are written in terms of their VEVs and the physical Higgs states as

$$\Phi_1 = \frac{1}{\sqrt{2}} \begin{pmatrix} \sqrt{2} (G^+ \cos \beta - H^+ \sin \beta) \\ v_1 - h \sin \alpha + H \cos \alpha + i (G \cos \beta - A \sin \beta) \end{pmatrix}, \quad (12)$$

$$\Phi_2 = \frac{1}{\sqrt{2}} \begin{pmatrix} \sqrt{2} (G^+ \sin \beta + H^+ \cos \beta) \\ v_2 + h \cos \alpha + H \sin \alpha + i (G \sin \beta + A \cos \beta) \end{pmatrix}, \quad (13)$$

where α is the mixing angle of the two CP-even Higgs bosons, $\tan\beta$ has been defined earlier and G and G^+ are the Goldstone bosons. The most general, CP-conserving potential for two Higgs doublets reads

$$\begin{aligned} \mathcal{V}_{2\text{HDM}} = & m_{11}^2 \Phi_1^\dagger \Phi_1 + m_{22}^2 \Phi_2^\dagger \Phi_2 - [m_{12}^2 \Phi_1^\dagger \Phi_2 + \text{h.c.}] \\ & + \frac{1}{2} \lambda_1 (\Phi_1^\dagger \Phi_1)^2 + \frac{1}{2} \lambda_2 (\Phi_2^\dagger \Phi_2)^2 + \lambda_3 (\Phi_1^\dagger \Phi_1) (\Phi_2^\dagger \Phi_2) + \lambda_4 (\Phi_1^\dagger \Phi_2) (\Phi_2^\dagger \Phi_1) \\ & + \left\{ \frac{1}{2} \lambda_5 (\Phi_1^\dagger \Phi_2)^2 + [\lambda_6 (\Phi_1^\dagger \Phi_1) + \lambda_7 (\Phi_2^\dagger \Phi_2)] \Phi_1^\dagger \Phi_2 + \text{h.c.} \right\}. \end{aligned} \quad (14)$$

Through the minimisation conditions of the Higgs potential above, m_{11}^2 and m_{22}^2 can be traded for the VEVs v_1 and v_2 , respectively. Furthermore, the tree-level mass relations allow the quartic coupling λ_{1-5} in Eq. (14) to be substituted by the four physical Higgs boson masses and the neutral sector mixing parameter $\sin(\beta - \alpha)$. Thus, in contrast with the SUSY models, in the 2HDMs the masses of the Higgs bosons are free input parameters, along with λ_6 , λ_7 , m_{12}^2 , $\sin(\beta - \alpha)$ and $\tan\beta$.

In the 2HDMs, the Yukawa couplings of the fermions are also *a priori* free parameters. However, depending on how the two Higgs doublets couple to the fermions, FCNCs can be mediated by scalars at the tree level. The requirement of no large FCNCs thus puts very strong restrictions on the coupling matrices. There are two general approaches for avoiding large FCNCs. One way is to impose a Z_2 symmetry so that each type of fermion only couples to one of the doublets (“natural flavour conservation”) [50, 51]. The same symmetry then holds also in the scalar potential (forcing $\lambda_6 = \lambda_7 = 0$), up to the soft breaking terms with parameter m_{12}^2 , thus further reducing the number of free parameters.

As noted in the Introduction, there are four ways of assigning the Z_2 charges, giving 2HDMs of Types I, II, X and Y. One defines as Type I the model where only the doublet Φ_2 couples to all fermions; Type II is the scenario similar to the MSSM, where Φ_2 couples to up-type quarks and Φ_1 couples to down-type quarks and leptons; in a Type X (or Type IV or ‘lepton-specific’) model Φ_2 couples to all quarks and Φ_1 couples to all leptons; and a Type Y (or Type III or ‘flipped’) model is built such that Φ_2 couples to up-type quarks and to leptons and Φ_1 couples to down-type quarks. The Type X and Type Y models have a similar phenomenology to Type I and II, respectively, especially in the context of this study. Specifically, $g_{qH^\pm}^2$ is the same in the Type I and Type X models. Similarly, the Type Y model has a similar Yukawa structure, and consequently $g_{qH^\pm}^2$, as Type II, except for the leptons which couple to a different Higgs doublet in either of the two models. This, incidentally, implies that there is no $\tan\beta$ -enhancement in the Type Y model to affect the $\text{BR}(H^\pm \rightarrow \tau\nu)$. We therefore consider only the Type I and Type II models, referred to as 2HDM-I and 2HDM-II, respectively, which are the most well-known ones.

Another way to achieve small FCNCs without imposing natural flavour conservation is to postulate that the Yukawa coupling matrices of the two Higgs doublets are proportional to each other, i.e., they are aligned. This approach has been adopted in the aforementioned A2HDM [28], where both scalar doublets (Φ_1 and Φ_2) couple to all types of fermions. In the Z_2 -symmetric 2HDMs discussed above the Yukawa couplings are determined solely by the parameter $\tan\beta$, while the CP-conserving A2HDM instead has separate parameters for the up-type quarks, the down-type quarks and the leptons, usually denoted by β^U , β^D and β^L . In the A2HDM there is no specific basis singled out by the fermionic sector due to the absence of the Z_2 symmetry. For this study we choose the basis where only one doublet acquires a VEV, called the ‘Higgs basis’. In this basis the input parameters include $\sin\alpha$ (where α is the angle that diagonalises the CP-even Higgs-sector), λ_2 , λ_3 , λ_7 and the above-mentioned alignment angles $\beta^{U,D,L}$, in addition to the physical Higgs boson masses.

The expressions for $g_{qH^\pm}^2$ in Eq. (1) for the different 2HDMs (including the A2HDM) are given

	2HDM-I	2HDM-II	A2HDM
$g_{qH^\pm}^2$	$m_b^2 \cot^2 \beta + m_t^2 \cot^2 \beta$	$m_b^2 \tan^2 \beta + m_t^2 \cot^2 \beta$	$m_b^2 \tan^2 \beta^D + m_t^2 \tan^2 \beta^U$

Table 1: The expressions for $g_{qH^\pm}^2$ in the different 2HDMs considered in this paper.

in Table 1. It should be noted that $g_{qH^\pm}^2$ in the 2HDM-II is identical to the one in the SUSY models.

4 Model scans and experimental constraints

We have performed scans of the parameter spaces of all the models considered here, requiring m_{H^\pm} to lie in the 200 GeV –500 GeV range. For each scenario except the MSSM, we carried out two separate scans for the cases with H_1 and H_2 alternatively playing the role of H_{obs} , i.e., having mass near 125 GeV and SM-like signal rates in the $\gamma\gamma$ and ZZ decay channels. We point out here that in the MSSM it is not possible to obtain a H with a mass around 125 GeV while also requiring $m_{H^\pm} \gtrsim 200$ GeV, as their masses lie very close to each other by theoretical construction. In the case of the SUSY models, since the masses of the scalar Higgs bosons are derived and not input parameters, we used the nested sampling package MultiNest-v2.18 [52] for efficiently scanning their parameter spaces.

The mass spectra and Higgs boson decay BRs for each scanned point of the MSSM, the NMSSM and the 2HDMs were computed using the public packages SUSY-HIT-v1.3 [53], NMSSMTools-v4.2.1 [54] and 2HDMC [55], respectively. For a point to be accepted in a given scan, it had to pass the condition $122 \text{ GeV} \leq m_{H_{\text{obs}}} \leq 128 \text{ GeV}$ for the SUSY models and $123 \text{ GeV} \leq m_{H_{\text{obs}}} \leq 127 \text{ GeV}$ in the 2HDMs. This is to take into account the experimental as well theoretical uncertainties (which are understandably larger in the presence of SUSY) in $m_{H_{\text{obs}}}$ predicted in the two scenarios. As for the b -physics observables, the points for which their theoretically evaluated values did not lie in the following ranges were rejected during the scans for the NMSSM and the A2HDM.

- $2.63 \times 10^{-4} \leq \text{BR}(\bar{B} \rightarrow X_s \gamma) \leq 4.23 \times 10^{-4}$,
- $0.71 \times 10^{-4} < \text{BR}(B_u \rightarrow \tau \nu) < 2.57 \times 10^{-4}$,
- $1.3 \times 10^{-9} < \text{BR}(B_s \rightarrow \mu^+ \mu^-) < 4.5 \times 10^{-9}$.

These 95% confidence level ranges are the ones suggested in the manual of the package SuperIso-v3.4 [56], which was used for the theoretical evaluation of these observables. Additionally, the scan points were also required to satisfy the constraint $\Delta M_{B_d} = (0.507 \pm 0.004) \text{ ps}^{-1}$, which is based on [57]. In the case of the Z_2 -symmetric 2HDMs, their parameter spaces consistent with the b -physics constraints were adopted directly from [57], so that these constraints were not tested against during the scans. Moreover, for SUSY models the (lightest) neutralino DM relic density was calculated for every point using the package MicrOMEGAs-v2.4.5 [58]. Only points with $\Omega_\chi h^2 < 0.131$, assuming a +10% theoretical error on the central value of 0.119 measured by the PLANCK collaboration [59], were retained.

Finally, we used the public package HiggsBounds-v4.1.3 [60] to test the neutral Higgs bosons other than the H_{obs} in a given case for each model against the exclusion limits from the Large Electron–Positron (LEP) collider, the Tevatron and the LHC. This program also takes care of the exclusion constraints on H^\pm from the various LHC searches mentioned in the Introduction. Finally,

the magnitude of a possible Higgs boson signal at the LHC is characterised by the signal strength modifier, defined as

$$\mu^X = \frac{\sigma(pp \rightarrow H_{\text{obs}} \rightarrow X)}{\sigma(pp \rightarrow h_{\text{SM}} \rightarrow X)}, \quad (15)$$

where X denotes the decay channel under consideration and h_{SM} denotes a 125 GeV SM Higgs boson. The theoretical counterparts of μ^X , which we refer to as R^X here, were obtained from the program HiggsSignals-v1.20 [61] for $X = \gamma\gamma, ZZ$.⁵ In our analysis below, while we will show all the good points from our scans, we will highlight the points for which $R^{\gamma\gamma, ZZ}$ are consistent with the measured $\mu^{\gamma\gamma, ZZ}$ at the LHC. The latest publicly available measurements read

$$\mu^{\gamma\gamma} = 1.13 \pm 0.24 \text{ and } \mu^{ZZ} = 1.0 \pm 0.29 \quad (16)$$

at CMS [62] and

$$\mu^{\gamma\gamma} = 1.57^{+0.33}_{-0.28} \text{ and } \mu^{ZZ} = 1.44^{+0.40}_{-0.35} \quad (17)$$

at ATLAS [63].⁶

5 Signal and background analysis

In addition to constraining the parameter spaces of the new physics models, knowledge of the mass of H_{obs} also provides an additional handle in identifying the $H^\pm \rightarrow W^\pm H_{\text{obs}}$ decay. We focus here on the decay $H_{\text{obs}} \rightarrow b\bar{b}$, as it generally has a substantial BR and allows for a full reconstruction of H_{obs} .⁷ In particular, we look for the production channel $pp \rightarrow t(b)H^\pm \rightarrow W^\mp b(b)W^\pm H_{\text{obs}}$, which, after semi-leptonic decays of the two W bosons and $H_{\text{obs}} \rightarrow b\bar{b}$, gives a final state of $bbb(b)jj\ell\nu_\ell$. The main background for this process is $t\bar{t}$ production, and here we consider all processes $pp \rightarrow t(b)W^\pm b\bar{b}$, where the extra pair of b -quarks can come from the emission of a gluon, a Higgs boson, or a Z . In this section we describe our method for reconstructing the H^\pm signal and separating it from the background events to give an estimate of the sensitivities that could be achieved at the 14 TeV LHC.

We generate the hard process for the signal using the MATCHIG package [6] with Pythia 6.4.28 [37], thus including the bg and gg contributions and subtracting the correct double-counting term to get proper b -jet momentum distributions. MadGraph5_aMC@NLO [65] is used to generate the backgrounds. Parton showers and hadronisation for both signal and background are performed with Pythia 8 [66], followed by detector simulation with DELPHES 3 [67] using experimental parameters calibrated to the ATLAS experiment with modified b -tagging efficiencies.⁸

For reconstruction and background reduction, we roughly follow the procedures of previous analyses [22], with the addition of a top veto (described below) to further suppress the background.

⁵The $\gamma\gamma$ and ZZ decay channels remain the only ones so far where a 5σ excess has been established at the LHC.

⁶We note here that the ATLAS collaboration has recently made public [64] an updated measurement, $\mu_{\gamma\gamma} = 1.17 \pm 0.27$, which is now comparatively much closer to the SM prediction. However, no updates on μ^{ZZ} for the same data set have been released. This implies that even if we use the newly released $\mu^{\gamma\gamma}$ value, the older and larger value of μ^{ZZ} in Eq. (17) will still rule out the corresponding model points, since R^{ZZ} is generally smaller than $R^{\gamma\gamma}$.

⁷This channel was also recently studied in [35], where it was noted that especially when uncertainties become dominated by systematics, the decay $H_{\text{obs}} \rightarrow \tau^+\tau^-$ can become more relevant due to its smaller backgrounds, despite a smaller BR and additional unobservable neutrinos. In this study, we consider only statistical uncertainties.

⁸The b -tagging used is given by $\epsilon_\eta \tanh(0.03p_T - 0.4)$, with the transverse momentum, p_T , in GeV, $\epsilon_\eta = 0.7$ for central ($|\eta| \leq 1.2$), and $\epsilon_\eta = 0.6$ for forward ($1.2 \leq |\eta| \leq 2.5$) jets. This choice is a conservative one in comparison with the ATLAS high-luminosity projections [68].

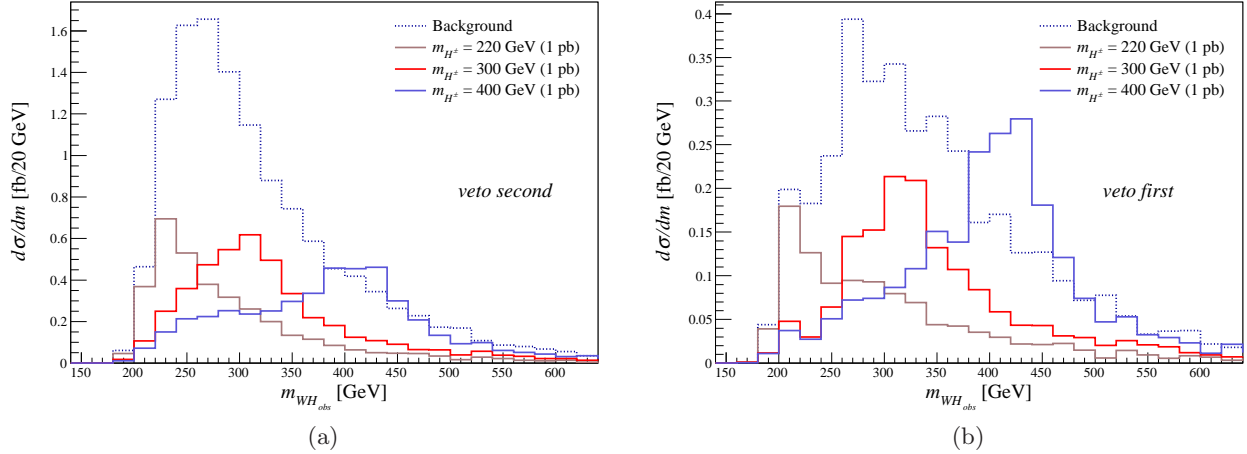


Figure 1: Reconstructed $m_{WH_{\text{obs}}}$ for signal and background with two different top vetos: (a) first identify an $H_{\text{obs}} \rightarrow b\bar{b}$ candidate, then veto event if two top jets can be reconstructed with remaining objects (veto second); (b) using all final state objects, veto event if two top jets can be reconstructed (veto first). The signal is normalised to $\sigma(pp \rightarrow tH^\pm) \times \text{BR}(H^\pm \rightarrow W^\pm H_{\text{obs}}) \times \text{BR}(H_{\text{obs}} \rightarrow b\bar{b}) = 1$ pb before selection and cuts.

1. Accept events with at least 3 b -jets, at least 2 light jets, one lepton (e or μ), and missing energy. All objects must have transverse momentum $p_T > 20$ GeV and rapidity $|\eta| \leq 2.5$, and must be separated from other objects by $\Delta R > 0.4$.
2. Find a hadronic W candidate from the light jets, taking the pair with the invariant mass m_{jj} closest to m_W . Reject the event if no pair satisfies $|m_{jj} - m_W| \leq 30$ GeV.
3. Reconstruct a leptonically decaying W using the lepton and the missing energy, by assuming that the missing energy comes entirely from the single neutrino and imposing the invariant mass constraint $m_{\ell\nu} = m_W$. Because this is a quadratic constraint, there is a two-fold ambiguity in the solution for the longitudinal momentum of the neutrino. If the solutions are real, both are kept, and if they are complex, the real part is kept as a single solution.
4. Apply top veto for high mass searches (“veto first”).
5. Find a Higgs boson candidate from the b -jets, taking the pair with the invariant mass m_{bb} closest to $m_{H_{\text{obs}}} \approx 125$ GeV. Reject the event if no pair satisfies $|m_{bb} - m_{H_{\text{obs}}}| \leq 15$ GeV.
6. Apply top veto for low mass searches (“veto second”).
7. Reconstruct a top quark using the remaining b -tagged jet(s) and reconstructed W ’s, taking the combination which gives m_{bW} closest to m_t . If one of the leptonically-decaying W solutions is selected here, the other is discarded. Reject the event if no combination satisfies $|m_{bW} - m_t| \leq 30$ GeV.
8. Reconstruct the charged Higgs candidate from the remaining W and the reconstructed H_{obs} to determine the discriminating variable $m_{WH_{\text{obs}}}$.

Because the largest background is by far $t\bar{t}X$, we wish to suppress it as much as possible by identifying events in which a top quark pair can be reconstructed. The majority of $t\bar{t}X$ events

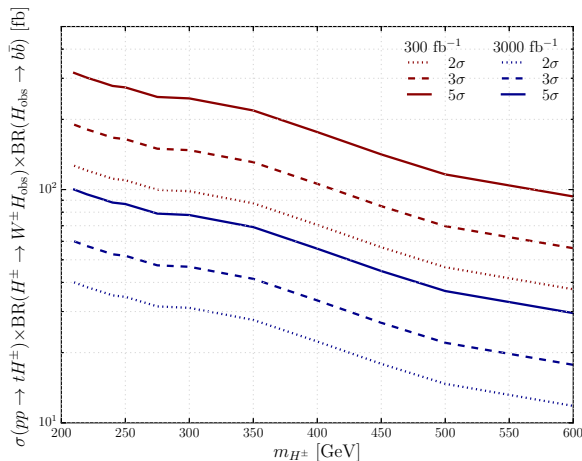


Figure 2: Sensitivity of the LHC to the signal cross section for exclusion, evidence and discovery, based on statistical uncertainties. Contours are thus shown for $S/\sqrt{B} = 2, 3, 5$ for an integrated luminosity of $\mathcal{L} = 300 \text{ fb}^{-1}$ at the next LHC run and at the high luminosity LHC with $\mathcal{L} = 3000 \text{ fb}^{-1}$, both at $\sqrt{s} = 14 \text{ TeV}$.

which are able to pass our requirement of providing an SM-like Higgs candidate do so by combining a b -jet coming from a top decay with another b -tagged jet, so the background will be most reduced if a top veto is applied before the Higgs reconstruction,

Veto first: Using reconstructed W 's and all remaining jets, veto event if two top quarks can be reconstructed, both with $|m_{Wj} - m_t| \leq 20 \text{ GeV}$.

We also wish to avoid unnecessarily cutting signal events. When a charged Higgs boson with $m_{H^\pm} \geq m_t$ undergoes the decay $H^\pm \rightarrow W^\pm H_{\text{obs}} \rightarrow W^\pm b\bar{b}$, it is kinematically possible for one of the b -jets from the H_{obs} decay to combine with the W to give an invariant mass close to the top mass. Indeed, this effect occurs in large regions of the available phase space for charged Higgs bosons with masses just above the threshold for $W^\pm H_{\text{obs}}$ decays. In this case, we wish to identify the $b\bar{b}$ pair from the H_{obs} decay before applying a top veto,

Veto second: After identifying two b -jets which reconstruct H_{obs} , using reconstructed W s and all remaining jets, veto event if two top quarks can be reconstructed, both with $|m_{Wj} - m_t| \leq 20 \text{ GeV}$.

Fig. 1(a) and (b) show the signal and background $m_{WH_{\text{obs}}}$ distributions for $m_{H^\pm} = 220, 300, 400 \text{ GeV}$ and the two types of top veto. The ‘‘veto first’’ scenario clearly reduces the background more effectively, but at the expense of a reduced signal. However, for larger m_{H^\pm} , the signal is less likely to fake an additional top, so there is less difference between the two vetoes in the higher mass signal distributions.

It is also clear from Fig. 1 that the H^\pm resonance can be reconstructed well enough to further separate it from the background. For each mass, we select a window in the reconstructed $m_{WH_{\text{obs}}}$ range which maximises the statistical significance S/\sqrt{B} of the signal.⁹ We additionally choose the top veto which maximises S/\sqrt{B} for each mass, and find that ‘‘veto second’’ is most effective

⁹In events where a leptonic W with two real solutions is used in the reconstruction, the event is accepted if either solution gives a $m_{WH_{\text{obs}}}$ within the window.

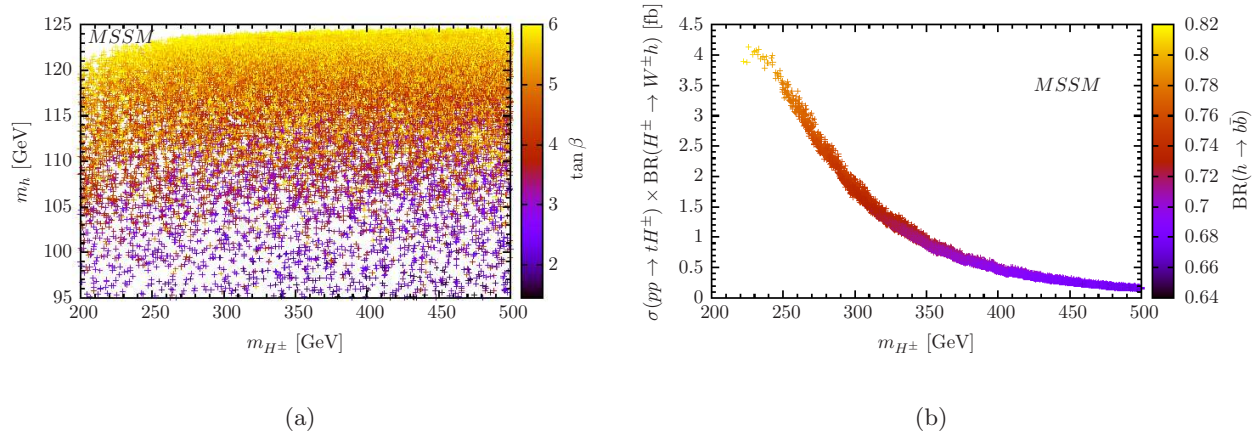


Figure 3: (a) m_h as a function of m_{H^\pm} in the MSSM, with the heat map showing the parameter $\tan\beta$. (b) $\sigma(pp \rightarrow tH^\pm) \times \text{BR}(H^\pm \rightarrow W^\pm H_{\text{obs}})$ as a function of m_{H^\pm} in the MSSM, with the heat map showing the $\text{BR}(H_{\text{obs}} \rightarrow b\bar{b})$.

at lower masses, $m_{H^\pm} \lesssim 350$ GeV, whereas “veto first” is preferable above this mass range.¹⁰ In Fig. 2 we show how this signal and background translate into sensitivities at the 14 TeV LHC for different values of the product $\sigma(pp \rightarrow tH^\pm) \times \text{BR}(H^\pm \rightarrow W^\pm H_{\text{obs}}) \times \text{BR}(H_{\text{obs}} \rightarrow b\bar{b})$, which we henceforth refer to as the signal cross section. We see that we can probe $\sigma \times \text{BR} \sim \mathcal{O}(100 \text{ fb})$ with an integrated luminosity of 300 fb^{-1} , but require higher luminosities to see $\mathcal{O}(10 \text{ fb})$ signals. These sensitivities can be compared to the model-dependent cross sections and BRs in various scenarios, which we discuss in the following section.

6 Results and discussion

6.1 MSSM

In Fig. 3(a) we show the mass of h as a function of m_{H^\pm} in the MSSM, with the heat map corresponding to $\tan\beta$. The ranges of the MSSM input parameters scanned to obtain these points are shown in Table 2(a). One sees in the figure that for the selected m_{H^\pm} range, $m_{H_{\text{SM}}}$ lying between 122 GeV – 128 GeV can only be obtained for $\tan\beta \gtrsim 6$. As noted earlier, such intermediate values of $\tan\beta$ bring down not only the $pp \rightarrow tH^\pm$ cross section but also the $\text{BR}(H^\pm \rightarrow W^\pm H_{\text{obs}})$. The product of these two quantities, only for points in the narrow strip corresponding to $m_{H_{\text{SM}}} > 122$ GeV and consequently to highest allowed $\tan\beta$ in Fig. 3(a), is shown in Fig. 3(b). This product hardly exceeds 4 fb, and that too only for points very close to the lower limit imposed on $m_{H_{\text{SM}}}$. The heat map in the figure shows the $\text{BR}(H_{\text{obs}} \rightarrow b\bar{b})$, which grows as the H_{obs} becomes more and more SM-like due to falling m_A , and hence m_{H^\pm} , given the intermediate value of $\tan\beta$.

6.2 NMSSM

Our initial scans for the NMSSM covered very wide ranges of the nine input parameters mentioned in Sec. 3. These scans revealed only a small region of the NMSSM-specific parameters where $m_{H_{\text{obs}}}$ and m_{H^\pm} both lied within the desired ranges. Two subsequent scans of this narrow region, for the

¹⁰As already mentioned, here we consider only statistical uncertainties (and give the significance as S/\sqrt{B}). A full experimental analysis with all errors included might prefer a different mass for the transition between vetoes.

MSSM parameter	Range
m_0 (GeV)	500 – 4000
$m_{1/2}$ (GeV)	300 – 2000
A_0 (GeV)	–7000 – 7000
μ (GeV)	100 – 2000
m_A (GeV)	100 – 500
$\tan \beta$	1 – 6

(a)

NMSSM parameter	Range
m_0 (GeV)	500 – 3000
$m_{1/2}$ (GeV)	300 – 2000
A_0 (GeV)	–4000 – 4000
$\tan \beta$	1 – 6
λ	0.45 – 0.7
κ	0.2 – 0.5
μ_{eff} (GeV)	100 – 200
A_λ (GeV)	0 – 500
A_κ (GeV)	–500 – 0

(b)

Table 2: Ranges of the input parameters scanned for (a) the MSSM and (b) the NMSSM.

cases with $H_{\text{obs}} = H_1$ and with $H_{\text{obs}} = H_2$ each, yielded a much larger density of interesting points. The corresponding parameter ranges are given in Table 2(b).

In Fig. 4(a) we show the $\text{BR}(H^\pm \rightarrow W^\pm H_{\text{obs}})$ as a function of m_{H^\pm} for the points obtained in the scan requiring H_1 to be the H_{obs} . In Fig. 4(b) the corresponding points for the case with $H_{\text{obs}} = H_2$ are shown. The heat maps in the two figures show the distribution of the $\sigma(pp \rightarrow tH^\pm)$. We see in the figures that while the $\text{BR}(H^\pm \rightarrow W^\pm H_{\text{obs}})$ in the $H_1 = H_{\text{obs}}$ ($H_2 = H_{\text{obs}}$) case can reach up to $\sim 23\%$ ($\sim 28\%$), its maximum reachable value drops slowly with decreasing m_{H^\pm} and, in fact, for $m_{H^\pm} < 250$ GeV it falls below 5%. This behaviour of the $\text{BR}(H^\pm \rightarrow W^\pm H_{\text{obs}})$ is thus in conflict with that of the $\sigma(pp \rightarrow tH^\pm)$, which clearly rises with decreasing m_{H^\pm} and is in fact maximal for points with the lowest $\text{BR}(H^\pm \rightarrow W^\pm H_{\text{obs}})$ observed.

In Fig. 5(a) we show the signal cross section for the case with $H_{\text{obs}} = H_1$. The points in green are the ones fulfilling only the b -physics constraints and we note for these points that, as a result of the tension between the $\text{BR}(H^\pm \rightarrow W^\pm H_{\text{obs}})$ and the $\sigma(pp \rightarrow tH^\pm)$, the total cross section barely exceeds 10 fb. The points in red and blue in the figure are the ones for which $R^{\gamma\gamma/ZZ}$ are consistent with the CMS and ATLAS ranges of $\mu^{\gamma\gamma/ZZ}$, respectively. Evidently, imposing these constraints further reduces the maximum signal cross section obtainable to below 5 fb. For the case with $H_{\text{obs}} = H_2$ the signal cross section, shown in Fig. 5(b), can reach slightly higher to around 20 pb, for the green points. This is owing to the somewhat larger $\text{BR}(H^\pm \rightarrow W^\pm H_{\text{obs}})$ obtainable for low m_{H^\pm} in this case compared to the $H_{\text{obs}} = H_1$ case. However, again the overall signal cross section is highly diminished for points observing the ATLAS or CMS signal rate constraints. Also shown in the Figs. 5(a) and (b) are the 2σ (exclusion), 3σ (evidence) and 5σ (discovery) sensitivity curves for 3000 fb^{-1} accumulated luminosity at the LHC 14 TeV run. All the good points from the scans lie well below the lowest (2σ) curve, implying that none of them has a signal cross section large enough to be testable even at such a high luminosity.

6.3 2HDM Types I and II

The scanned ranges of the parameters in these two models are shown in Table 3. Note that in the 2HDM-II, $m_{H^\pm} \lesssim 320$ GeV is excluded for all values of $\tan \beta$ by the constraint on $\text{BR}(\bar{B} \rightarrow X_s \gamma)$, while $\tan \beta \lesssim 1.5$ is ruled out for m_{H^\pm} up to 500 GeV or so by the ΔM_{B_d} constraint, according to [57]. We therefore reduced the input range of m_{H^\pm} instead of imposing these constraints during

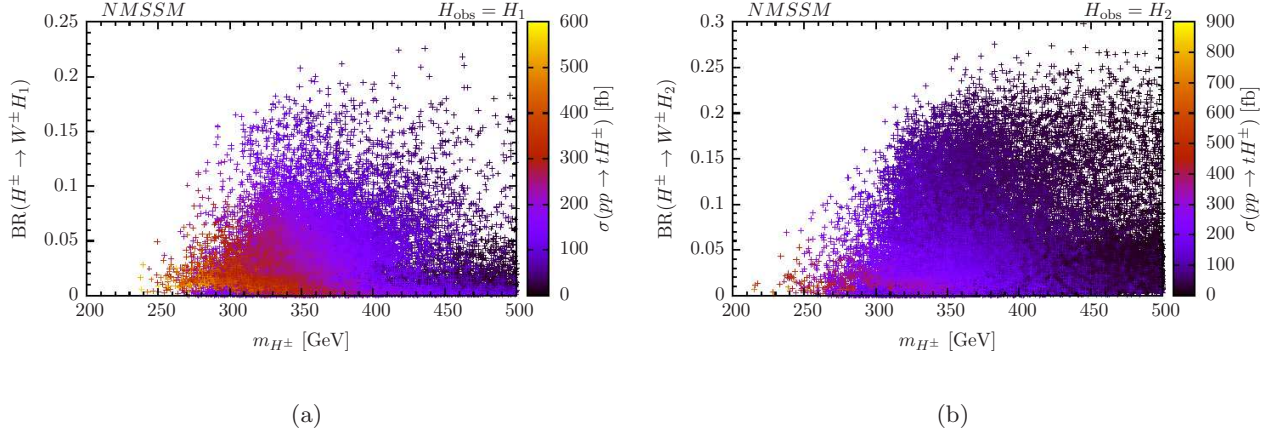


Figure 4: $\text{BR}(H^\pm \rightarrow W^\pm H_{\text{obs}})$ as a function of m_{H^\pm} in the NMSSM when (a) $H_{\text{obs}} = H_1$ and (b) $H_{\text{obs}} = H_2$, with the heat map showing the $\sigma(pp \rightarrow tH^\pm)$.

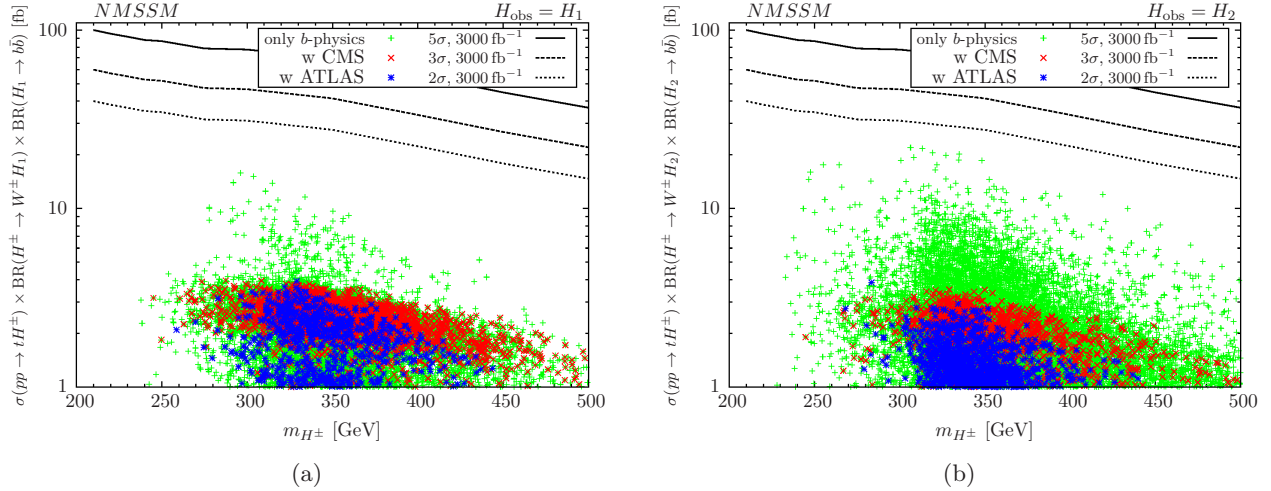


Figure 5: Signal cross section as a function of m_{H^\pm} in the NMSSM when (a) $H_{\text{obs}} = H_1$ and (b) $H_{\text{obs}} = H_2$. See text for details.

the scans for this model. The $\text{BR}(H^\pm \rightarrow W^\pm H_{\text{obs}})$ for 2HDM-I with the $H_{\text{obs}} = h$ case, shown in Fig. 6(a), can be as high as $\sim 95\%$ for a fairly large number of points. Moreover, compared to the NMSSM, while the maximum $\sigma(pp \rightarrow tH^\pm)$ reachable is much lower here, the $\text{BR}(H^\pm \rightarrow W^\pm H_{\text{obs}})$ grows much more sharply with increasing m_{H^\pm} . As a result, there are plenty of low m_{H^\pm} points where both the $\text{BR}(H^\pm \rightarrow W^\pm H_{\text{obs}})$ as well as the $\sigma(pp \rightarrow tH^\pm)$, shown by the heat map, can be significant. In Fig. 6(b) are shown the corresponding quantities for the $H_{\text{obs}} = H$ case in the 2HDM-I. In this case a very large $\text{BR}(H^\pm \rightarrow W^\pm H_{\text{obs}})$ is obtainable for a comparatively much smaller number of points and it mostly stays below 40%.

In Fig. 7(a) we show the signal cross section for the $H_{\text{obs}} = h$ case in the 2HDM-I as a function of m_{H^\pm} . The colour convention for the points in all the figures showing the signal cross section henceforth is the same as in Fig. 5. We note that, owing to the much larger $\text{BR}(H^\pm \rightarrow W^\pm H_{\text{obs}})$

Parameter	2HDM-I		2HDM-II	
	$H_{\text{obs}} = h$	$H_{\text{obs}} = H$	$H_{\text{obs}} = h$	$H_{\text{obs}} = H$
m_h (GeV)	123 – 127	80 – 115	123 – 127	80 – 115
m_H (GeV)	135 – 500	123 – 127	135 – 500	123 – 127
$m_{H^\pm} = m_A$ (GeV)	135 – 500		320 – 500	
$\tan \beta$	1.5 – 6			
$ \sin(\beta - \alpha) $	0 – 1			
m_{12}^2 (GeV ²)	$0 - m_A^2 \cos \beta \sin \beta$			

Table 3: Ranges of the input parameters scanned for the 2HDM Types I and II.

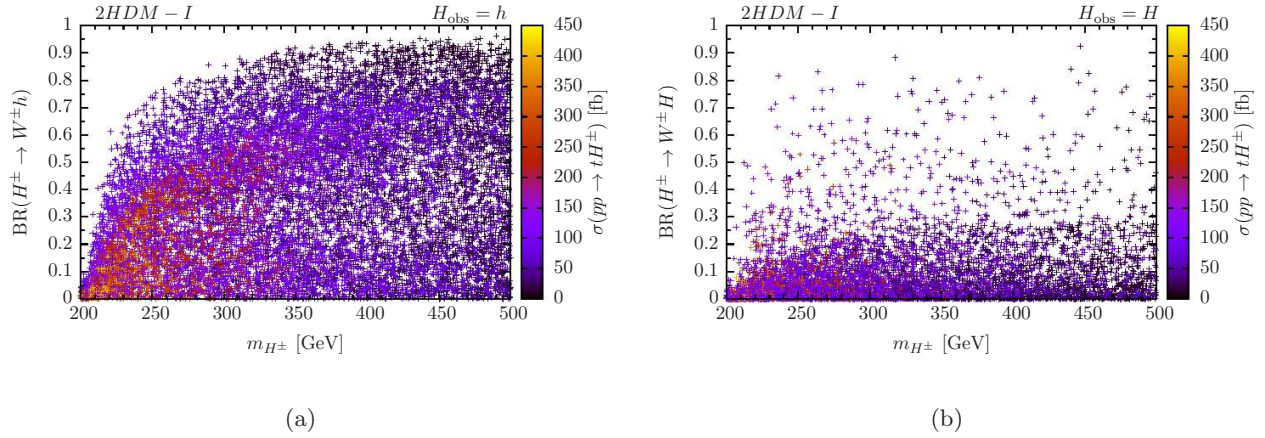


Figure 6: $\text{BR}(H^\pm \rightarrow W^\pm H_{\text{obs}})$ as a function of m_{H^\pm} in the 2HDM-I when (a) $H_{\text{obs}} = h$ and (b) $H_{\text{obs}} = H$, with the heat map showing the $\sigma(pp \rightarrow tH^\pm)$.

generally obtainable in this model compared to the NMSSM, the total cross section can reach as high as about 100 fb. A small portion of the green points with $m_{H^\pm} > 400$ GeV lies above the 2σ sensitivity curve corresponding to $\mathcal{L} = 300 \text{ fb}^{-1}$ and should thus be reachable at the LHC. The picture, however, becomes grim when the LHC signal rate constraints are imposed. Points consistent with the CMS constraints have a maximum possible cross section of around 20 fb, while none of the points obtained in the scans are able to satisfy the ATLAS constraints.

Turning to the 2HDM-II, for the $H_{\text{obs}} = h$ case one sees in Fig. 8(a) that in this model both the $\text{BR}(H^\pm \rightarrow W^\pm H_{\text{obs}})$ and the $\sigma(pp \rightarrow tH^\pm)$ show a similar behaviour as noted in the 2HDM-I above, being significantly large simultaneously for a number of points with m_{H^\pm} up to ~ 400 GeV. The maximum obtainable values of both these quantities are also similar to those in the 2HDM-I. In the $H_{\text{obs}} = H$ case the $\text{BR}(H^\pm \rightarrow W^\pm H_{\text{obs}})$ struggles to reach high values generally and in fact stays close to 0 for a vast majority of the points, as seen in Fig. 8(b). In Figs. 9(a) and (b) we show the signal cross sections for the $H_{\text{obs}} = h$ and $H_{\text{obs}} = H$ cases, respectively, in the 2HDM-II. In the former case, not only do a large number of points observing only the b -physics constraints lie above the 5σ sensitivity curve for $\mathcal{L} = 3000 \text{ fb}^{-1}$, but also some of the points consistent with the CMS constraints can have a signal cross section in excess of 30 fb and should thus be accessible at the

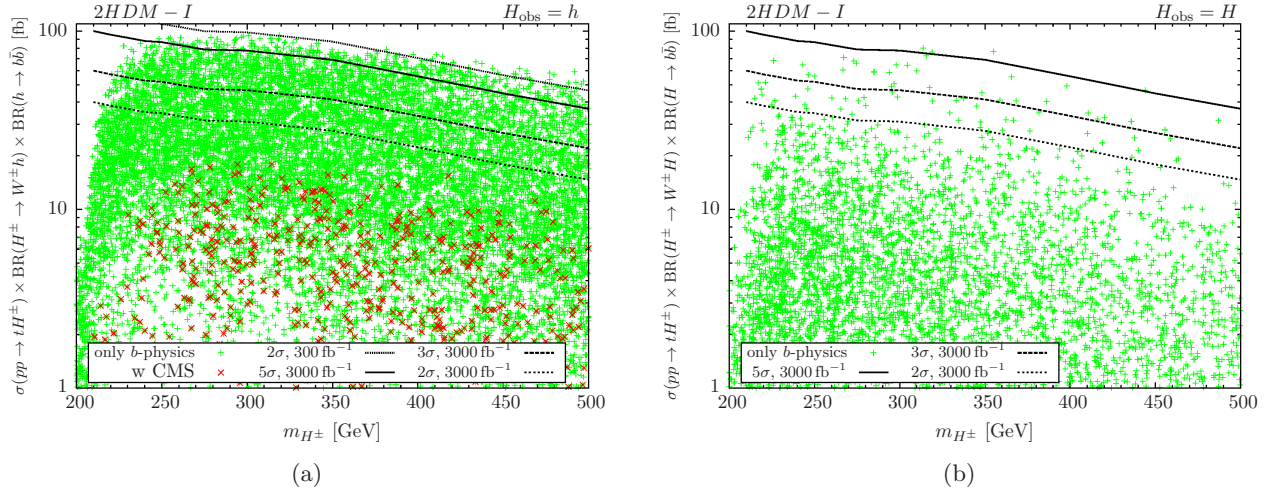


Figure 7: Signal cross section as a function of m_{H^\pm} in the 2HDM-I when (a) $H_{\text{obs}} = h$ and (b) $H_{\text{obs}} = H$. See text for details.

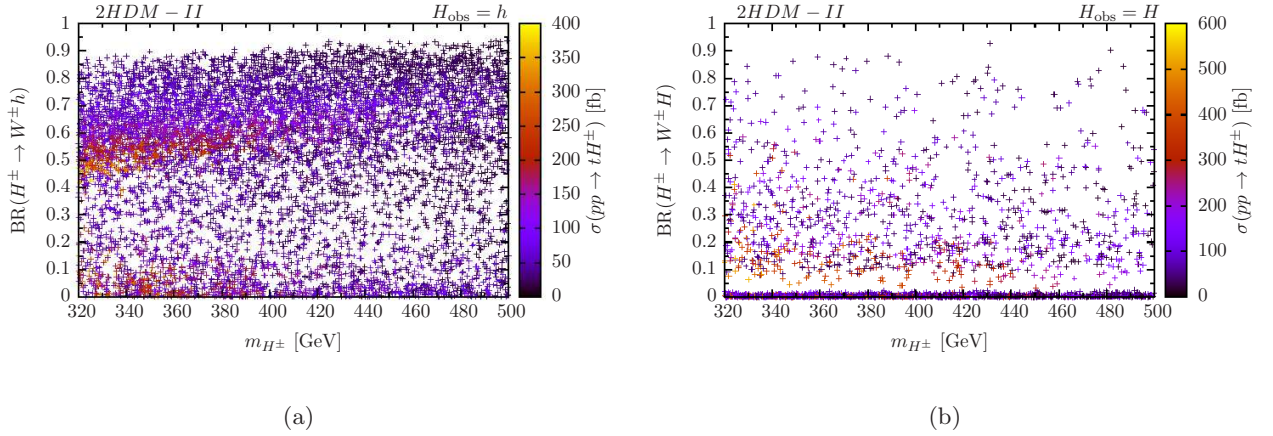


Figure 8: $\text{BR}(H^\pm \rightarrow W^\pm H_{\text{obs}})$ as a function of m_{H^\pm} in the 2HDM-II when (a) $H_{\text{obs}} = h$ and (b) $H_{\text{obs}} = H$, with the heat map showing the $\sigma(pp \rightarrow tH^\pm)$.

LHC. In the $H_{\text{obs}} = H$ case, however, the maximum reachable cross section for points consistent with the CMS and ATLAS signal rate constraints barely exceeds 10 fb and 1.5 fb, respectively, only when m_{H^\pm} is below 350 GeV or so.

6.4 A2HDM

The scanned ranges of the A2HDM parameters are given in Table 4 and have been adopted from [69]. In Fig. 10(a) we show the $\text{BR}(H^\pm \rightarrow W^\pm H_{\text{obs}})$ for the $H_{\text{obs}} = h$ case, which can reach unity over the entire desired mass range of H^\pm . Also, the $\sigma(pp \rightarrow tH^\pm)$, illustrated by the heat map in the figure, can reach the pb level, but it is maximal only for points for which the $\text{BR}(H^\pm \rightarrow W^\pm H_{\text{obs}})$ is relatively small, $\lesssim 40\%$. On the other hand, Fig. 10(b) shows that in the $H_{\text{obs}} = H$ case the $\text{BR}(H^\pm \rightarrow W^\pm H_{\text{obs}})$ mostly stays below $\sim 35\%$.

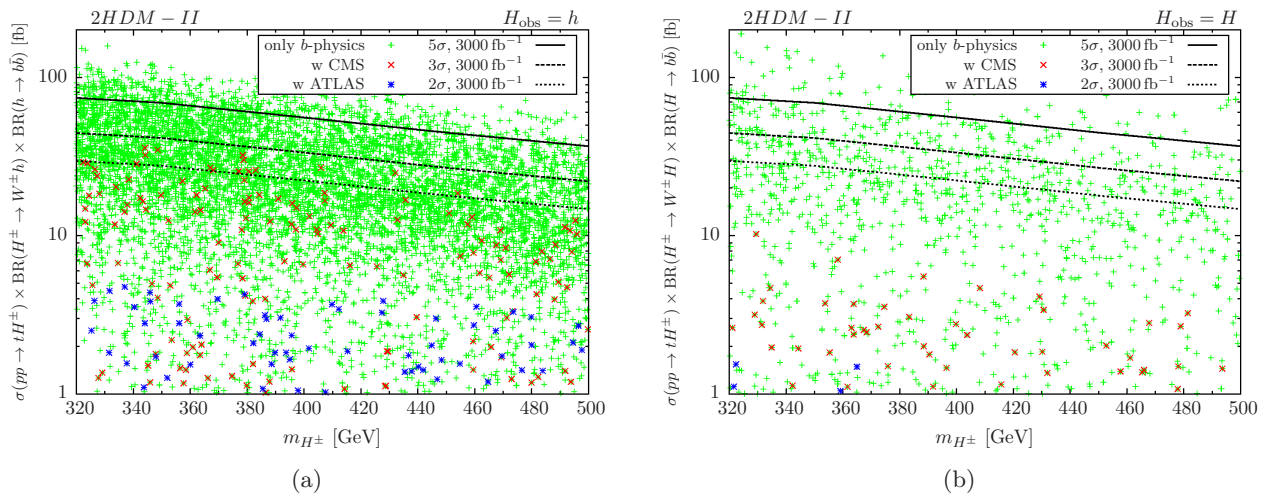


Figure 9: Signal cross section as a function of m_{H^\pm} in the 2HDM-II when (a) $H_{\text{obs}} = h$ and (b) $H_{\text{obs}} = H$. See text for details.

Parameter	$H_{\text{obs}} = h$	$H_{\text{obs}} = H$
m_h (GeV)	123 – 127	80 – 115
m_H (GeV)	135 – 300	123 – 127
$m_{H^\pm} = m_A$ (GeV)	200 – 500	
$ \sin \alpha $	0 – 1	
λ_2	0 – 4π	
λ_3	$-\sqrt{\lambda_1 \lambda_2} - 4\pi$	
$ \lambda_7 $	0 – 4π	
$ \beta^{U,D,L} $	0 – 1.57	

Table 4: Ranges of the input parameters scanned for the A2HDM.

In Fig. 11(a) the signal cross section for the $H_{\text{obs}} = h$ case is shown. This cross section can reach much higher, ~ 700 fb, than in the ordinary 2HDMs, when the constraints from the LHC Higgs boson searches are not imposed. Points with such a high cross section lie above even the 5σ sensitivity curve for the LHC with $\mathcal{L} = 3000 \text{ fb}^{-1}$. This implies that the H^\pm in this model could be discoverable at the standard luminosity LHC over almost the entire mass range analysed for this channel. However, as in the other models above, points satisfying the LHC constraints have a much smaller signal cross section generally. Still, unlike in any of the other models considered here, a small number of points consistent with the CMS constraints lies above the 5σ sensitivity curve for $\mathcal{L} = 3000 \text{ fb}^{-1}$ and could thus be visible at the high luminosity LHC. The same is not true though for the $H_{\text{obs}} = H$ case, seen in Fig. 11(b), where only a couple of points consistent with the CMS constraints appear to be testable at the high luminosity LHC.

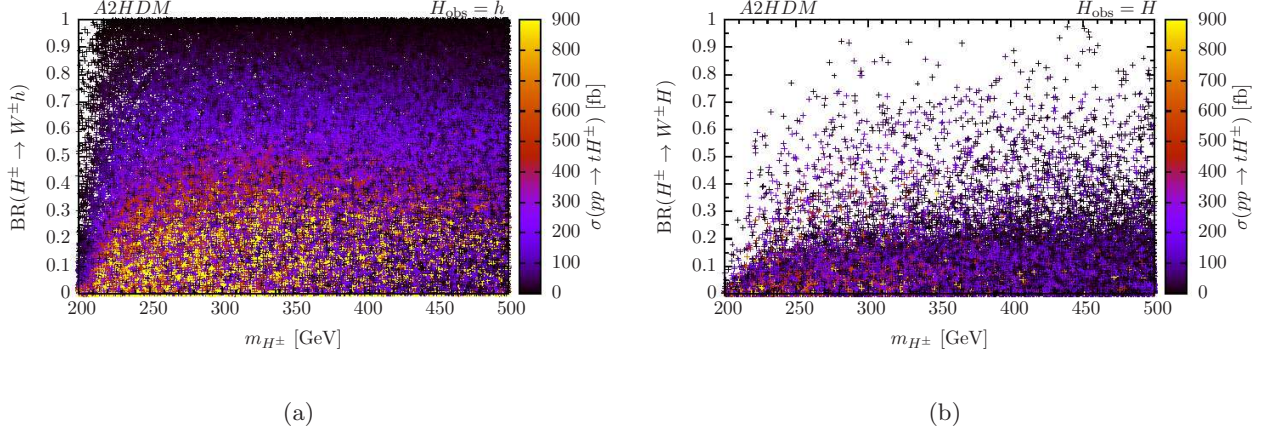


Figure 10: $\text{BR}(H^\pm \rightarrow W^\pm H_{\text{obs}})$ as a function of m_{H^\pm} in the A2HDM when (a) $H_{\text{obs}} = h$ and (b) $H_{\text{obs}} = H$, with the heat map showing the $\sigma(pp \rightarrow tH^\pm)$.

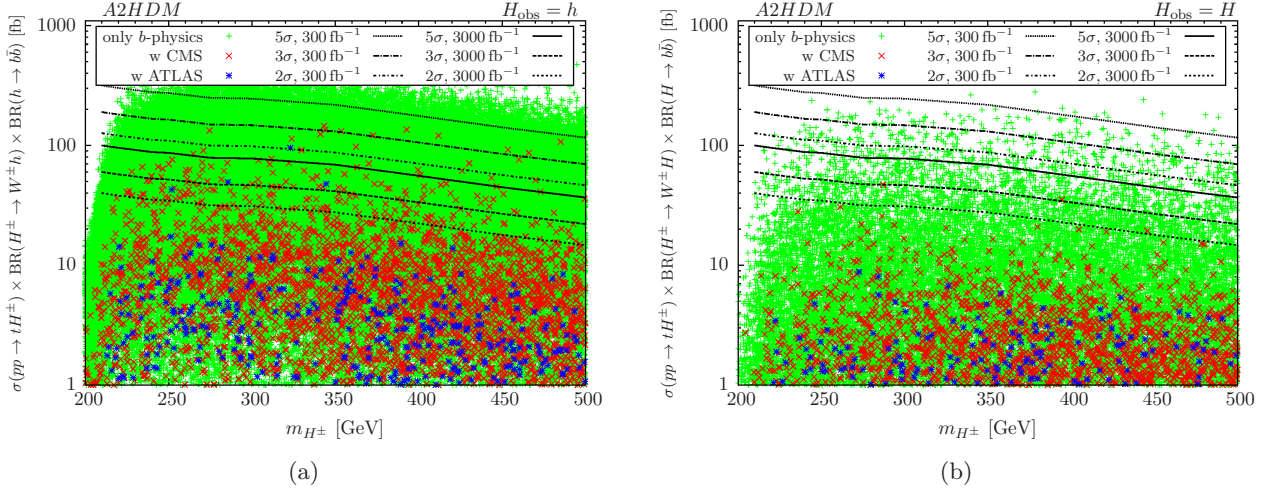


Figure 11: Signal cross section as a function of m_{H^\pm} in the A2HDM when (a) $H_{\text{obs}} = h$ and (b) $H_{\text{obs}} = H$. See text for details.

7 Conclusions

In this article we have analysed the detectability of H^\pm in the WH_{obs} decay mode in some minimal extensions of the SM, at the upcoming Run 2 of the LHC with $\sqrt{s} = 14$ TeV. We have discussed some important features of the models of our interest, in particular the coupling parameters governing the production of H^\pm in pp collisions as well as the $H^\pm \rightarrow WH_{\text{obs}}$ decay process. We have performed dedicated scans of the parameter spaces of these models to search for their regions where a H^\pm with a mass lying in the 200 GeV – 500 GeV range can be obtained and its production cross section can be maximised. These scans were subject to the most relevant constraints from b -physics, from the LHC Higgs boson searches and, in the case of SUSY models, from relic density measurements. Moreover, in the NMSSM as well as in the 2HDMs we considered both the possibilities of the observed Higgs boson being the lightest or the next-to-lightest CP-even scalar of the

model.

We then reconstructed the signal and the background in the $bbb(b)jj\ell\nu_\ell$ final state and, through a dedicated detector-level analysis, estimated the signal significance for various accumulated luminosities at the LHC. We found that, through a judicious choice of selection criteria, including a veto on $t\bar{t}$ events and the requirement of a reconstructed 125 GeV Higgs boson from a pair of b -tagged jets, we were able to significantly reduce the backgrounds. The semi-leptonic channel provides enough kinematic information to reconstruct the m_{H^\pm} peak and identify signals with $\sigma(pp \rightarrow tH^\pm) \times \text{BR}(H^\pm \rightarrow W^\pm H_{\text{obs}}) \times \text{BR}(H_{\text{obs}} \rightarrow b\bar{b}) \sim \mathcal{O}(100 \text{ fb})$ with an integrated luminosity of 300 fb^{-1} , with even better sensitivity at high luminosities.

We have concluded that in the SUSY models studied here, the $H^\pm \rightarrow WH_{\text{obs}}$ decay channel does not carry as much promise for the identification of a H^\pm as has been envisaged in some earlier studies. This is due to the fact that the $pp \rightarrow H^\pm$ production process and the subsequent $H^\pm \rightarrow WH_{\text{obs}}$ decay process generally show contrasting dependence on the various parameters involved. The situation looks a bit better in the Z_2 -symmetric 2HDMs, as long as the constraints from the LHC measurements of the Higgs boson signal rates are ignored. Imposing these constraints leaves an insignificant number of points in the 2HDM-II visible at only the high luminosity ($\sim 3000 \text{ fb}^{-1}$) LHC, implying that the Higgs boson assumed to be the one observed at the LHC in these scenarios deviates substantially from SM-like properties. In the case of the A2HDM, a fairly large portion of the parameter space could in general be tested even at the standard luminosity ($\sim 300 \text{ fb}^{-1}$) LHC. However, again if the measurements of the observed Higgs boson signal rates do not fluctuate much from the current ones, only a few parameter space points lie within the reach of the LHC at this luminosity.

ACKNOWLEDGEMENTS

This work was in part funded by the Swedish Research Council under contracts 2007-4071 and 621-2011-5107. The work of S. Moretti has been funded in part through the NExT Institute. The computational work was in part carried out on resources provided by the Swedish National Infrastructure for Computing (SNIC) at Uppsala Multidisciplinary Center for Advanced Computational Science (UPPMAX) under Projects p2013257 and SNIC 2014/1-5.

References

- [1] A. Djouadi, “The Anatomy of electro-weak symmetry breaking. II. The Higgs bosons in the minimal supersymmetric model,” *Phys.Rept.* **459** (2008) 1–241, [arXiv:hep-ph/0503173](#) [hep-ph].
- [2] F. Maltoni, Z. Sullivan, and S. Willenbrock, “Higgs-boson production via bottom-quark fusion,” *Phys.Rev.* **D67** (2003) 093005, [arXiv:hep-ph/0301033](#) [hep-ph].
- [3] E. Boos and T. Plehn, “Higgs boson production induced by bottom quarks,” *Phys.Rev.* **D69** (2004) 094005, [arXiv:hep-ph/0304034](#) [hep-ph].
- [4] S. Moretti, “Improving the discovery potential of charged Higgs bosons at the Tevatron and Large Hadron Collider,” *Pramana* **60** (2003) 369–376, [arXiv:hep-ph/0205104](#) [hep-ph].
- [5] K. Assamagan, M. Guchait, and S. Moretti, “Charged Higgs bosons in the transition region $M_{H^\pm} \sim m_t$ at the LHC,” [arXiv:hep-ph/0402057](#) [hep-ph].

- [6] J. Alwall and J. Rathsman, “Improved description of charged Higgs boson production at hadron colliders,” *JHEP* **0412** (2004) 050, [arXiv:hep-ph/0409094](#) [hep-ph].
- [7] J. Alwall, C. Biscarat, S. Moretti, J. Rathsman, and A. Sopczak, “The $pp/pp\bar{p} \rightarrow tbH^\pm$ process at the Tevatron in HERWIG and PYTHIA simulations,” *Eur.Phys.J.* **C39S1** (2005) 37–39, [arXiv:hep-ph/0312301](#) [hep-ph].
- [8] S.-h. Zhu, “Complete next-to-leading order QCD corrections to charged Higgs boson associated production with top quark at the CERN large hadron collider,” *Phys.Rev.* **D67** (2003) 075006, [arXiv:hep-ph/0112109](#) [hep-ph].
- [9] T. Plehn, “Charged Higgs boson production in bottom gluon fusion,” *Phys.Rev.* **D67** (2003) 014018, [arXiv:hep-ph/0206121](#) [hep-ph].
- [10] J. Gunion, H. Haber, F. Paige, W.-K. Tung, and S. Willenbrock, “Neutral and Charged Higgs Detection: Heavy Quark Fusion, Top Quark Mass Dependence and Rare Decays,” *Nucl.Phys.* **B294** (1987) 621.
- [11] K. A. Assamagan and N. Gollub, “The ATLAS discovery potential for a heavy charged Higgs boson in $gg \rightarrow tbH^\pm$ with $H^\pm \rightarrow tb$,” *Eur.Phys.J.* **C39S2** (2005) 25–40, [arXiv:hep-ph/0406013](#) [hep-ph].
- [12] S. Lowette, J. D’Hondt, and P. Vanlaer, “Charged MSSM Higgs boson observability in the $H^\pm \rightarrow tb$ decay,” Tech. Rep. CERN-CMS-NOTE-2006-109, CERN, 2006
- [13] V. D. Barger, R. Phillips, and D. Roy, “Heavy charged Higgs signals at the LHC,” *Phys.Lett.* **B324** (1994) 236–240, [arXiv:hep-ph/9311372](#) [hep-ph]. ; J. Gunion, “Detecting the t b decays of a charged Higgs boson at a hadron supercollider,” *Phys.Lett.* **B322** (1994) 125–130, [arXiv:hep-ph/9312201](#) [hep-ph].
- [14] D. Miller, S. Moretti, D. Roy, and W. J. Stirling, “Detecting heavy charged Higgs bosons at the CERN LHC with four b quark tags,” *Phys.Rev.* **D61** (2000) 055011, [arXiv:hep-ph/9906230](#) [hep-ph]. ; S. Moretti and D. Roy, “Detecting heavy charged Higgs bosons at the LHC with triple b tagging,” *Phys.Lett.* **B470** (1999) 209–214, [arXiv:hep-ph/9909435](#) [hep-ph].
- [15] K. Odagiri, “Searching for heavy charged Higgs bosons in the tau-neutrino decay mode at LHC,” [arXiv:hep-ph/9901432](#) [hep-ph]. ; S. Raychaudhuri and D. Roy, “Sharpening up the charged Higgs boson signature using τ polarization at LHC,” *Phys.Rev.* **D53** (1996) 4902–4908, [arXiv:hep-ph/9507388](#) [hep-ph].
- [16] B. Bullock, K. Hagiwara, and A. D. Martin, “Tau polarization as a signal of charged Higgs bosons,” *Phys.Rev.Lett.* **67** (1991) 3055–3057. ; B. Bullock, K. Hagiwara, and A. D. Martin, “Tau polarization and its correlations as a probe of new physics,” *Nucl.Phys.* **B395** (1993) 499–533.
- [17] D. Roy, “The Hadronic τ decay signature of a heavy charged Higgs boson at LHC,” *Phys.Lett.* **B459** (1999) 607–614, [arXiv:hep-ph/9905542](#) [hep-ph].
- [18] CMS Collaboration, “Search for a heavy charged Higgs boson in proton-proton collisions at $\sqrt{s} = 8$ TeV with the CMS detector,” Tech. Rep. CMS-PAS-HIG-13-026, 2014

- [19] CMS Collaboration, “Search for charged Higgs bosons with the H^\pm to tau nu decay channel in the fully hadronic final state at $\sqrt{s} = 8$ TeV,” Tech. Rep. CMS-PAS-HIG-14-020, 2014
- [20] ATLAS collaboration, “Search for charged Higgs bosons decaying via $H^\pm \rightarrow \tau^\pm \nu$ in hadronic final states using pp collision data at $\sqrt{s} = 8$ TeV with the ATLAS detector,” Tech. Rep. ATLAS-CONF-2014-050, ATLAS-COM-CONF-2014-071, 2014
- [21] ATLAS Collaboration, G. Aad *et al.*, “Search for a light charged Higgs boson in the decay channel $H^\pm \rightarrow c\bar{s}$ in $t\bar{t}$ events using pp collisions at $\sqrt{s} = 7$ TeV with the ATLAS detector,” *Eur.Phys.J.* **C73** (2013) 2465, arXiv:1302.3694 [hep-ex].
- [22] M. Drees, M. Guchait, and D. Roy, “Signature of charged to neutral Higgs boson decay at the LHC in SUSY models,” *Phys.Lett.* **B471** (1999) 39–44, arXiv:hep-ph/9909266 [hep-ph]. ; S. Moretti, “The $W^\pm h$ decay channel as a probe of charged Higgs boson production at the large hadron collider,” *Phys.Lett.* **B481** (2000) 49–56, arXiv:hep-ph/0003178 [hep-ph].
- [23] A. Sopczak, “Higgs boson searches at LEP up to $\sqrt{s} = 202$ GeV,” arXiv:hep-ph/0004015 [hep-ph].
- [24] A. Djouadi and J. Quevillon, “The MSSM Higgs sector at a high M_{SUSY} : reopening the low $\tan\beta$ regime and heavy Higgs searches,” *JHEP* **1310** (2013) 028, arXiv:1304.1787 [hep-ph].
- [25] CMS Collaboration, S. Chatrchyan *et al.*, “Observation of a new boson at a mass of 125 GeV with the CMS experiment at the LHC,” *Phys.Lett.* **B716** (2012) 30–61, arXiv:1207.7235 [hep-ex]. ; ATLAS Collaboration, G. Aad *et al.*, “Observation of a new particle in the search for the Standard Model Higgs boson with the ATLAS detector at the LHC,” *Phys.Lett.* **B716** (2012) 1–29, arXiv:1207.7214 [hep-ex].
- [26] U. Ellwanger, “A Higgs boson near 125 GeV with enhanced di-photon signal in the NMSSM,” *JHEP* **1203** (2012) 044, arXiv:1112.3548 [hep-ph]. ; S. King, M. Muhlleitner, and R. Nevzorov, “NMSSM Higgs Benchmarks Near 125 GeV,” *Nucl.Phys.* **B860** (2012) 207–244, arXiv:1201.2671 [hep-ph]. ; J. Cao *et al.*, “A SM-like Higgs near 125 GeV in low energy SUSY: a comparative study for MSSM and NMSSM,” *JHEP* **1203** (2012) 086, arXiv:1202.5821 [hep-ph]. ; U. Ellwanger and C. Hugonie, “Higgs bosons near 125 GeV in the NMSSM with constraints at the GUT scale,” *Adv.High Energy Phys.* **2012** (2012) 1, arXiv:1203.5048 [hep-ph]. ; T. Gherghetta, B. von Harling, A. D. Medina, and M. A. Schmidt, “The Scale-Invariant NMSSM and the 126 GeV Higgs Boson,” *JHEP* **1302** (2013) 032, arXiv:1212.5243 [hep-ph].
- [27] G. Branco, P. Ferreira, L. Lavoura, M. Rebelo, M. Sher, *et al.*, “Theory and phenomenology of two-Higgs-doublet models,” *Phys.Rept.* **516** (2012) 1–102, arXiv:1106.0034 [hep-ph].
- [28] A. Pich and P. Tuzon, “Yukawa Alignment in the Two-Higgs-Doublet Model,” *Phys.Rev.* **D80** (2009) 091702, arXiv:0908.1554 [hep-ph].
- [29] M. Bisset, M. Guchait, and S. Moretti, “Signatures of MSSM charged Higgs bosons via chargino neutralino decay channels at the LHC,” *Eur.Phys.J.* **C19** (2001) 143–154, arXiv:hep-ph/0010253 [hep-ph]. ; M. Bisset, F. Moortgat, and S. Moretti, “Trilepton + top signal from chargino neutralino decays of MSSM charged Higgs bosons at the LHC,” *Eur.Phys.J.* **C30** (2003) 419–434, arXiv:hep-ph/0303093 [hep-ph].

- [30] A. Belyaev, R. Guedes, S. Moretti, and R. Santos, “Very Light Higgs Bosons in Extended Models at the LHC,” *Phys.Rev.* **D81** (2010) 095006, arXiv:0912.4150 [hep-ph]. ; M. Aoki, R. Guedes, S. Kanemura, S. Moretti, R. Santos, *et al.*, “Light Charged Higgs bosons at the LHC in 2HDMs,” *Phys.Rev.* **D84** (2011) 055028, arXiv:1104.3178 [hep-ph].
- [31] A. Akeroyd, S. Moretti, and J. Hernandez-Sanchez, “Light charged Higgs bosons decaying to charm and bottom quarks in models with two or more Higgs doublets,” *Phys.Rev.* **D85** (2012) 115002, arXiv:1203.5769 [hep-ph]. ; A. Akeroyd, S. Moretti, and J. Hernandez-Sanchez, “ $H^\pm \rightarrow cb$ in models with two or more Higgs doublets,” arXiv:1409.7596 [hep-ph].
- [32] P. B. Dev and A. Pilaftsis, “Maximally Symmetric Two Higgs Doublet Model with Natural Standard Model Alignment,” *JHEP* **1412** (2014) 024, arXiv:1408.3405 [hep-ph]. ; A. Broggio, E. J. Chun, M. Passera, K. M. Patel, and S. K. Vempati, “Limiting two-Higgs-doublet models,” *JHEP* **1411** (2014) 058, arXiv:1409.3199 [hep-ph].
- [33] W.-S. Hou and R. Willey, “Effects of Charged Higgs Bosons on the Processes $b \rightarrow s$ Gamma, $b \rightarrow s g^*$ and $b \rightarrow s$ Lepton+ Lepton-,” *Phys.Lett.* **B202** (1988) 591. ; T. G. Rizzo, “ $b \rightarrow s\gamma$ in the Two Higgs Doublet Model,” *Phys.Rev.* **D38** (1988) 820. ; B. Grinstein, R. P. Springer, and M. B. Wise, “Effective Hamiltonian for Weak Radiative B Meson Decay,” *Phys.Lett.* **B202** (1988) 138. ; B. Grinstein, R. P. Springer, and M. B. Wise, “Strong Interaction Effects in Weak Radiative \bar{B} Meson Decay,” *Nucl.Phys.* **B339** (1990) 269–309. ; F. Borzumati and C. Greub, “2HDMs predictions for anti-B \rightarrow X(s) gamma in NLO QCD,” *Phys.Rev.* **D58** (1998) 074004, arXiv:hep-ph/9802391 [hep-ph]. ; F. Borzumati and C. Greub, “Two Higgs doublet model predictions for anti-B \rightarrow X(s) gamma in NLO QCD: Addendum,” *Phys.Rev.* **D59** (1999) 057501, arXiv:hep-ph/9809438 [hep-ph]. ; M. Misiak, H. Asatrian, K. Bieri, M. Czakon, A. Czarnecki, *et al.*, “Estimate of $B\bar{B} \rightarrow X_s\gamma$ at $O(\alpha_s^2)$,” *Phys.Rev.Lett.* **98** (2007) 022002, arXiv:hep-ph/0609232 [hep-ph].
- [34] M. Jung, A. Pich, and P. Tuzon, “Charged-Higgs phenomenology in the Aligned two-Higgs-doublet model,” *JHEP* **1011** (2010) 003, arXiv:1006.0470 [hep-ph]. ; M. Jung, A. Pich, and P. Tuzon, “The B \rightarrow Xs gamma Rate and CP Asymmetry within the Aligned Two-Higgs-Doublet Model,” *Phys.Rev.* **D83** (2011) 074011, arXiv:1011.5154 [hep-ph]. ; M. Jung, X.-Q. Li, and A. Pich, “Exclusive radiative B-meson decays within the aligned two-Higgs-doublet model,” *JHEP* **1210** (2012) 063, arXiv:1208.1251 [hep-ph]. ; G. Cree and H. E. Logan, “Yukawa alignment from natural flavor conservation,” *Phys.Rev.* **D84** (2011) 055021, arXiv:1106.4039 [hep-ph].
- [35] B. Coleppa, F. Kling, and S. Su, “Charged Higgs Search via AW^\pm/HW^\pm Channel,” arXiv:1408.4119 [hep-ph].
- [36] F. Borzumati, J.-L. Kneur, and N. Polonsky, “Higgs-Strahlung and R-parity violating slepton-Strahlung at hadron colliders,” *Phys.Rev.* **D60** (1999) 115011, arXiv:hep-ph/9905443 [hep-ph].
- [37] T. Sjöstrand, S. Mrenna, and P. Z. Skands, “PYTHIA 6.4 Physics and Manual,” *JHEP* **0605** (2006) 026, arXiv:hep-ph/0603175 [hep-ph].
- [38] M. Klasen, K. Kovarik, P. Nason, and C. Weydert, “Associated production of charged Higgs bosons and top quarks with POWHEG,” *Eur.Phys.J.* **C72** (2012) 2088, arXiv:1203.1341 [hep-ph].

- [39] P. Nason, “A New method for combining NLO QCD with shower Monte Carlo algorithms,” *JHEP* **0411** (2004) 040, [arXiv:hep-ph/0409146 \[hep-ph\]](#). ; S. Frixione, P. Nason, and C. Oleari, “Matching NLO QCD computations with Parton Shower simulations: the POWHEG method,” *JHEP* **0711** (2007) 070, [arXiv:0709.2092 \[hep-ph\]](#). ; S. Alioli, P. Nason, C. Oleari, and E. Re, “A general framework for implementing NLO calculations in shower Monte Carlo programs: the POWHEG BOX,” *JHEP* **1006** (2010) 043, [arXiv:1002.2581 \[hep-ph\]](#).
- [40] C. Weydert, S. Frixione, M. Herquet, M. Klasen, E. Laenen, *et al.*, “Charged Higgs boson production in association with a top quark in MC@NLO,” *Eur.Phys.J.* **C67** (2010) 617–636, [arXiv:0912.3430 \[hep-ph\]](#).
- [41] S. Frixione and B. R. Webber, “Matching NLO QCD computations and parton shower simulations,” *JHEP* **0206** (2002) 029, [arXiv:hep-ph/0204244 \[hep-ph\]](#).
- [42] S. Moretti, K. Odagiri, P. Richardson, M. H. Seymour, and B. R. Webber, “Implementation of supersymmetric processes in the HERWIG event generator,” *JHEP* **0204** (2002) 028, [arXiv:hep-ph/0204123 \[hep-ph\]](#).
- [43] M. Guchait and S. Moretti, “Improving the discovery potential of charged Higgs bosons at Tevatron run II,” *JHEP* **0201** (2002) 001, [arXiv:hep-ph/0110020 \[hep-ph\]](#).
- [44] <https://twiki.cern.ch/twiki/bin/view/CMSPublic/PhysicsResultsHIG>;
<https://twiki.cern.ch/twiki/bin/view/AtlasPublic/HiggsPublicResults>
- [45] P. Fayet, “Supergauge Invariant Extension of the Higgs Mechanism and a Model for the electron and Its Neutrino,” *Nucl.Phys.* **B90** (1975) 104–124. ; J. R. Ellis, J. Gunion, H. E. Haber, L. Roszkowski, and F. Zwirner, “Higgs Bosons in a Nonminimal Supersymmetric Model,” *Phys.Rev.* **D39** (1989) 844.
- [46] L. Durand and J. L. Lopez, “Upper Bounds on Higgs and Top Quark Masses in the Flipped SU(5) x U(1) Superstring Model,” *Phys.Lett.* **B217** (1989) 463. ; M. Drees, “Supersymmetric Models with Extended Higgs Sector,” *Int.J.Mod.Phys.* **A4** (1989) 3635.
- [47] D. Miller, R. Nevzorov, and P. Zerwas, “The Higgs sector of the next-to-minimal supersymmetric standard model,” *Nucl.Phys.* **B681** (2004) 3–30, [arXiv:hep-ph/0304049 \[hep-ph\]](#).
- [48] U. Ellwanger, C. Hugonie, and A. M. Teixeira, “The Next-to-Minimal Supersymmetric Standard Model,” *Phys.Rept.* **496** (2010) 1–77, [arXiv:0910.1785 \[hep-ph\]](#).
- [49] M. Maniatis, “The Next-to-Minimal Supersymmetric extension of the Standard Model reviewed,” *Int.J.Mod.Phys.* **A25** (2010) 3505–3602, [arXiv:0906.0777 \[hep-ph\]](#).
- [50] S. L. Glashow and S. Weinberg, “Natural Conservation Laws for Neutral Currents,” *Phys. Rev.* **D15** (1977) 1958.
- [51] E. Paschos, “Diagonal Neutral Currents,” *Phys.Rev.* **D15** (1977) 1966.
- [52] F. Feroz, M. Hobson, and M. Bridges, “MultiNest: an efficient and robust Bayesian inference tool for cosmology and particle physics,” *Mon.Not.Roy.Astron.Soc.* **398** (2009) 1601–1614, [arXiv:0809.3437 \[astro-ph\]](#).

- [53] A. Djouadi, M. Muhlleitner, and M. Spira, “Decays of supersymmetric particles: The Program SUSY-HIT (SUSpect-SdecaY-Hdecay-InTerface),” *Acta Phys.Polon.* **B38** (2007) 635–644, [arXiv:hep-ph/0609292](#) [hep-ph].
- [54] <http://www.th.u-psud.fr/NMHDECAY/nmssmtools.html>
- [55] D. Eriksson, J. Rathsmann, and O. Stål, “2HDMC: Two-Higgs-Doublet Model Calculator Physics and Manual,” *Comput.Phys.Commun.* **181** (2010) 189–205, [arXiv:0902.0851](#) [hep-ph].
- [56] A. Arbey and F. Mahmoudi, “SuperIso Relic: A program for calculating relic density and flavor physics observables in Supersymmetry,” *Comput.Phys.Commun.* **176** (2007) 367–382, [arXiv:0906.0369](#) [hep-ph].
- [57] F. Mahmoudi and O. Stål, “Flavor constraints on the two-Higgs-doublet model with general Yukawa couplings,” *Phys.Rev.* **D81** (2010) 035016, [arXiv:0907.1791](#) [hep-ph].
- [58] G. Belanger, F. Boudjema, A. Pukhov, and A. Semenov, “micrOMEGAs2.0: a program to calculate the relic density of dark matter in a generic model,” *Comput.Phys.Commun.* **181** (2010) 1277–1292, [arXiv:hep-ph/0607059](#) [hep-ph].
- [59] Planck Collaboration , P. Ade *et al.*, “Planck 2013 results. XVI. Cosmological parameters,” *Astron.Astrophys.* **571** (2014) A16, [arXiv:1303.5076](#) [astro-ph.CO].
- [60] P. Bechtle, O. Brein, S. Heinemeyer, G. Weiglein, and K. E. Williams, “HiggsBounds: Confronting Arbitrary Higgs Sectors with Exclusion Bounds from LEP and the Tevatron,” *Comput.Phys.Commun.* **181** (2010) 138–167, [arXiv:0811.4169](#) [hep-ph]. ; P. Bechtle, O. Brein, S. Heinemeyer, G. Weiglein, and K. E. Williams, “HiggsBounds 2.0.0: Confronting Neutral and Charged Higgs Sector Predictions with Exclusion Bounds from LEP and the Tevatron,” *Comput.Phys.Commun.* **182** (2011) 2605–2631, [arXiv:1102.1898](#) [hep-ph]. ; P. Bechtle, O. Brein, S. Heinemeyer, O. Stål, T. Stefaniak, *et al.*, “Recent Developments in HiggsBounds and a Preview of HiggsSignals,” *PoS CHARGED2012* (2012) 024, [arXiv:1301.2345](#) [hep-ph]. ; P. Bechtle, O. Brein, S. Heinemeyer, O. Stål, T. Stefaniak, *et al.*, “HiggsBounds – 4: Improved Tests of Extended Higgs Sectors against Exclusion Bounds from LEP, the Tevatron and the LHC,” *Eur.Phys.J.* **C74** (2014) 2693, [arXiv:1311.0055](#) [hep-ph].
- [61] P. Bechtle, S. Heinemeyer, O. Stål, T. Stefaniak, and G. Weiglein, “*HiggsSignals*: Confronting arbitrary Higgs sectors with measurements at the Tevatron and the LHC,” *Eur.Phys.J.* **C74** (2014) 2711, [arXiv:1305.1933](#) [hep-ph].
- [62] CMS Collaboration, “Precise determination of the mass of the higgs boson and studies of the compatibility of its couplings with the standard model,” Tech. Rep. CMS-PAS-HIG-14-009, CERN, Geneva, Jul, 2014.
- [63] ATLAS Collaboration, “Updated coupling measurements of the higgs boson with the atlas detector using up to 25 fb^{-1} of proton-proton collision data,” Tech. Rep. ATLAS-CONF-2014-009, CERN, Geneva, May, 2014.
- [64] ATLAS Collaboration , G. Aad *et al.*, “Measurement of Higgs boson production in the diphoton decay channel in pp collisions at center-of-mass energies of 7 and 8 TeV with the ATLAS detector,” [arXiv:1408.7084](#) [hep-ex].

- [65] J. Alwall, R. Frederix, S. Frixione, V. Hirschi, F. Maltoni, *et al.*, “The automated computation of tree-level and next-to-leading order differential cross sections, and their matching to parton shower simulations,” *JHEP* **1407** (2014) 079, [arXiv:1405.0301](#) [[hep-ph](#)].
- [66] T. Sjostrand, S. Mrenna, and P. Z. Skands, “A Brief Introduction to PYTHIA 8.1,” *Comput.Phys.Commun.* **178** (2008) 852–867, [arXiv:0710.3820](#) [[hep-ph](#)].
- [67] DELPHES 3 , J. de Favereau *et al.*, “DELPHES 3, A modular framework for fast simulation of a generic collider experiment,” *JHEP* **1402** (2014) 057, [arXiv:1307.6346](#) [[hep-ex](#)].
- [68] ATLAS Collaboration, “Performance assumptions based on full simulation for an upgraded ATLAS detector at a High-Luminosity LHC,” Tech. Rep. ATL-PHYS-PUB-2013-009, CERN, Geneva, Sep, 2013.
- [69] R. Enberg, J. Rathsman, and G. Wouda, “Higgs phenomenology in the Stealth Doublet Model,” [arXiv:1311.4367](#) [[hep-ph](#)].